Asymmetry effects in homodyne-like measurements: Gaussian approximation and positive operator-valued measures

A. S. Naumchik,[1, *] Roman K. Goncharov,[1, †] and Alexei D. Kiselev[2, 3, ‡]

[1]*ITMO University, Kronverksky Pr. 49, Saint Petersburg 197101, Russia*
[2]*Laboratory of Quantum Processes and Measurements,*
ITMO University, Kadetskaya Line 3b, Saint Petersburg 199034, Russia
[3]*Leading Research Center "National Center for Quantum Internet",*
ITMO University, Birzhevaya Line 16, Saint Petersburg 199034, Russia
(Dated: July 29, 2025)

We study applicability of the Gaussian approximation describing photon count statistics for both the homodyne and the double homodyne measurements in the presence of asymmetry effects when the beam splitters are unbalanced and the quantum efficiencies of the photodetectors are not identical. We also use the Gaussian approximation to construct the positive operator-valued measure (POVM) that takes into account the asymmetry effects. It is found that, when the Skellam distribution is approximated using the asymptotic expansions of modified Bessel functions for large argument, the asymmetry effects lead to ill-posed Gaussian POVM.

I. INTRODUCTION

Homodyne measurement is an important example of Gaussian measurements and is widely applied in continuous-variable quantum key distribution (CV-QKD) systems [1–6]. This measurement traditionally involves a beam splitter (BS), where the two input ports are occupied by the signal and reference modes, and the two output ports are detected by quantum detectors (see Fig. 1). To simplify calculations, one can consider the reference mode to be much stronger in amplitude than the signal, leading to the so-called strong Local Oscillator (LO) approximation. For the resulting statistical distribution to accurately describe a real physical process, it is necessary to construct the corresponding positive-valued operator measure (POVM).

Balanced homodyne: In Ref. [7] a study of potential benefits of using weak LO (of same amplitude as signal) is conducted. Description is focused on correlation functions, and considers 2 schemes: homodyne intensity correlation scheme, consisting of 2 BS, the intensity correlations are measured with 2 photodetectors, and homodyne cross correlation scheme with 1 BS (not 50 : 50). These schemes are of particular interest in cases where low overall efficiencies prevent the detection of phase-sensitive effects by standard balanced or unbalanced homodyning. Strong LO does not allow for observing squeezing effect, and LO noise is not balanced out. Small classical excess noise of the LO is amplified when its strong, so detection of squeezed light is not possible. On the contrary, using weak LO, relative squeezing is much larger and therefore easier to observe, new phase-sensitive effects can be observed as well: the normally ordered intensity variance, the normally ordered field strength variance, and the normally ordered correlation of the intensity and field strength fluctuations. The corresponding spectral properties can be recorded by the homodyne correlation schemes: the spectrum of intensity fluctuations, the squeezing spectrum, the correlation spectrum of field strength and intensity fluctuations. Last one gives the spectral correlation of two noncommuting observables. And decreasing LO results in lesser classical noise. Detectors must be of high efficiency to detect these signals, and signals need to be temporally stable. Balanced homodyning is insensitive to local-oscillator quadrature-phase noise and hence provides (1) a means of detecting reduced quadrature-phase fluctuations (squeezing) that is perhaps more practical than one-port homodyning and (2) an output signal-to-noise ratio that can be a modest to significant improvement over that of unbalanced homodyning and direct detection [8]. In addition to the unavoidable quantum fluctuations, it is shown that excess noise from the local oscillator always affects homodyning and, when it is broadband, also heterodyning. Both the quantum and the excess noise of the local oscillator can be eliminated by coherent subtraction of the two outputs of a 50/50 beam splitter [9]. Excess intensity noise in the local oscillator can be canceled [10].

Unbalanced: Ref. [11] discusses the technique of unbalanced homodyne detection (only one output port of the BS is detected). It shows that reconstructing the quantum state of the signal field from the photo-counting statistics recorded in this scheme (related to s-parametrized quasiprobability distributions) is possible for $s < 1$. To do so, POVM is derived. Practically this is difficult to realize: the noise is significant, presently available photomultipliers have small efficiencies, so that the applicability of the method might be presently limited to the reconstruction of smooth quasiprobability distributions. A possible solution is to use of an array of highly efficient avalanche photodiodes instead of photon count detectors [11, 12]. Naturally, theoretical description (photon count formula) is to be modified as well

[13, 14] to account for number of detectors (and dark photon counts). Quality of the results of reconstruction are affected by quantum detector efficiency, being less accurate for lower efficiencies.

Double homodyne: Ref. [15] discusses the the double homodyne scheme with finite LO intensity. The paper demonstrates how the eight-port detector can be used to reconstruct the quantum state of the signal field, even when the LO intensity is not significantly larger than the signal. Analysis of limits of weak LO and strong LO is given as well: for strong LO they obtain the Q-function of the signal state, and for weak LO the phase is lost and they only able to measure the probability distribution for the photon number. Classical treatment of the homodyne is given as well.

LO of other states: In Ref. [16], Schrödinger cat states (even and odd) of finite amplitude are considered as local oscillators of a standard homodyne scheme. Since LO state is not Gaussian, this measurement scheme is not Gaussian as well. This scheme allows for preparation of non-Gaussian states..

In the context of **quantum random number generators** (QRNGs), accounting for measurement imperfections is of great importance for ensuring the reliability and security of the generated random numbers. As demonstrated in Ref. [17], classical noise plays a significant role in influencing the entropy of the random numbers generated, as well as leading to potential vulnerabilities, as it can be tampered with. Our results suggest that homodyne measurement imperfections are alike to classical noise in the sense of affecting the variance of the output, meaning similar conclusions of the performance of QRNG may be drawn.

For ideal homodyne and double homodyne detection schemes with unequal detector efficiencies, POVMs are well-known, being the projectors onto quadrature operators and superposition of these projectors, respectively. However, practical applications have imperfections [18]. Although accounting for BS imbalance in the formulae is conceptually simple, the calculations have not been carried out explicitly. Additionally, similar projectorsconsiderations have not been applied to the double homodyne scheme. Considering photon-counting schemes, detection imperfections are not only losses, but photon number resolution [19, 20] and detector dead time [19, 21]. These imperfections are beyond the scope of this work.

Critical cases of asymmetry in homodyne scheme were discussed previously. Ref. [11] discusses the technique of unbalanced homodyne detection (in the sense of only one quantum detector used as opposed to traditionally detecting both output ports of BS). It shows that reconstructing the quantum state of the signal field from the photocounting statistics recorded in this scheme (related to s-parametrized quasiprobability distributions) is possible. Quality of the results of reconstruction are affected by quantum detector efficiency, being less accurate for lower efficiencies. However, this scheme is difficult to realize, as the effect of classical noise is significant, and presently available photomultipliers have small efficiencies, so that the applicability of the method might be limited. A possible solution is to use of an array of highly efficient avalanche photodiodes instead of photon count detectors [11, 12]. Naturally, theoretical description (photon count formula) is to be modified as well [13, 14]. These studies focus on the critical case of imbalance (one of the detector ports being unused) for specific measurement purposes. In this sense, the case with an unused port can be interpreted as corresponding to zero efficiency.

Numerical studies of photon count distributions for different signal states in homodyne schemes have been performed [22]. In that work, photon difference distributions for Fock signal states were analyzed, and the dependency on detector efficiencies was studied. However, the dependency of the quality of the LO approximation compared to the exact distribution was not quantified. A numerical study on the role of the LO intensity in an imperfect homodyne scheme has been conducted in Ref. [23]. In this scheme, the homodyne setup has non-unity, equal quantum detectors and a balanced BS. It shows that a strong LO is not required to reconstruct a quantum state; a low-intensity LO can provide a reconstruction with sufficient fidelity, which increases as the LO intensity increases.

Device imperfections play a significant role in continuous-variable quantum key distribution (CV-QKD). In Ref. [24] a CV-QKD system is modeled numerically using a classical description of electromagnetic fields to investigate the impact of device imperfections on the secure key rate. Specifically, a non-ideal beam splitter and an unbalanced detector are considered. The study reveals that these imperfections lead to a reduction in the secure key generation rate. However, this analysis is based on a classical, rather than quantum, description of the system, which may limit the accuracy of the results.

Our analysis focuses on the case of an unbalanced beam splitter and unequal non-unity quantum efficiency of photodetectors, which we refer to as the asymmetrical case, in contrast to the traditionally studied symmetrical case of a balanced beam splitter and equal non-unity quantum efficiencies. To obtain the approximation, we approximate the Poisson distribution with the Gaussian distribution, which will be referred to as Gaussian approximation. We will use the LO approximation to further simplify the resulting function. After this, we construct the respective POVM and numerically study the quality of the approximation. We apply developed formalism to another homodyne-based detection scheme, namely double homodyne scheme (also known as heterodyne scheme in the QKD literature [5, 6, 25]), to demonstrate its applicability. We find that for the asymmetrical double homodyne POVM an extension to the set of squeezed coherent states is required. The results for asymmetrical measurements are then used to calculate the CV-QKD
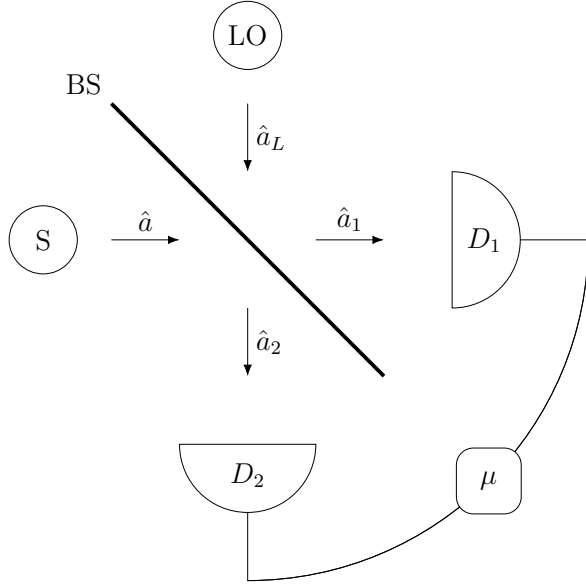
Figure 1: Scheme of a homodyne receiver: S is the source of the signal mode with the annihilation operator $\hat{a}$, LO is the source of the reference mode (local oscillator) with the annihilation operator $\hat{a}_L$, and BS is the beam splitter with the amplitude transmission and reflection coefficients $t = \cos\theta$ and $r = \sin\theta$, respectively; photodetectors D_1 and D_2 have quantum efficiencies η_1 and η_2, and $\mu \equiv m_1 - m_2$ is the photon count difference.

asymptotic secret fraction to estimate the impact of measurement asymmetry on protocol security.

Our findings also reveal that the usual approach of approximating the Skellam distribution using the asymptotic expansion of the modified Bessel function of the first kind is not applicable in the asymmetrical case.

The paper is organized as follows. In Sec. II we obtain the statistical distribution of difference photon counts in Gaussian approximation, from which we obtain the respective POVM. We thoroughly analyze the dependence of the statistical distribution on the asymmetry parameters. In Sec. III we conduct the analysis of the double homodyne scheme analogously to the previous section, finding out that the resulting POVM is not well defined for all asymmetry parameters, requiring generalization. In Sec. IV we generalize the double homodyne POVM to the set of squeezed coherent states. In Sec. V we apply our results for homodyne and double homodyne detection to calculate the asymptotic secret fraction for an ideal CV-QKD system. Finally, in Sec. VI we conclude the paper with a brief summary of the results and suggestions for future development.

II. HOMODYNE DETECTION

A. Gaussian approximation

We begin with brief discussion of the homodyne measurement setup schematically depicted in Fig. 1. To this end, we assume that the beam spitter is unbalanced and its scattering matrix is chosen to be a real-valued rotation matrix with the transmission and reflection amplitudes, t and r, given by

$$t = \cos\theta \equiv C, \quad r = \sin\theta \equiv S. \tag{1}$$

Then the input coherent states of the signal mode and the local oscillator are transformed into the output coherent states as follows

$$|\alpha, \alpha_L\rangle \mapsto |\alpha_1, \alpha_2\rangle, \tag{2}$$
$$\alpha_1 = C\alpha + S\alpha_L, \quad \alpha_2 = -S\alpha + C\alpha_L, \tag{3}$$

so that the joint probability of m_1 and m_2 photon counts for the photodetectors D_1 and D_2 can be computed from the well-known Kelley-Kleiner formula [26] (see also Ref. [27]):

$$\mathsf{P}(m_1, m_2) = \langle \alpha_1, \alpha_2 | : \prod_{l=1}^{2} \frac{(\eta_l \hat{n}_l)^{m_l} e^{-\eta_l \hat{n}_l}}{m_l!} : |\alpha_1, \alpha_2\rangle$$
$$= \prod_{l=1}^{2} \frac{(\eta_l |\alpha_l|^2)^{m_l}}{m_l!} e^{-\eta_l |\alpha_l|^2} \tag{4}$$

where $: \ldots :$ stands for normal ordering, index $l \in \{1, 2\}$ labels output ports of the beam splitter, $\hat{n}_l = \hat{a}_l^\dagger \hat{a}_l$ is the photon number operator, m_l is the number of photon counts, η_l is the quantum efficiency of the detector D_l.

We can now introduce the photon count difference

$$\mu = m_1 - m_2 \tag{5}$$

so that its statistical distribution can be written in the form of a product of the two Poisson distributions as follows

$$\mathsf{P}(\mu) = \sum_{m_2 = \max(0, -\mu)}^{\infty} \frac{(\eta_1 |\alpha_1|^2)^{\mu + m_2}}{(\mu + m_2)!} e^{-\eta_1 |\alpha_1|^2}$$
$$\times \frac{(\eta_2 |\alpha_2|^2)^{m_2}}{m_2!} e^{-\eta_2 |\alpha_2|^2}. \tag{6}$$

It is well known that, by performing summation over m_2, the probabilty $\mathsf{P}(\mu)$ reduces to the Skellam distribution given by [28]

$$\mathsf{P}(\mu) = e^{-\eta_1 |\alpha_1|^2} e^{-\eta_2 |\alpha_2|^2} \left(\frac{\eta_1 |\alpha_1|^2}{\eta_2 |\alpha_2|^2} \right)^{\mu/2}$$
$$\times I_\mu \big(2\sqrt{\eta_1 \eta_2 |\alpha_1|^2 |\alpha_2|^2} \big), \tag{7}$$

where $I_k(z)$ is the modified Bessel function of the first kind [29].

An important point is that, at sufficiently large $|\alpha_1|$ and $|\alpha_2|$, Poisson distributions that enter Eq. (4) can be approximated using the probability density functions of the normal distributions with mean and variance both equal to the mean of the corresponding Poisson distribution, $\lambda_i = \eta_i|\alpha_i|^2$. Then, in the continuum limit where summation in Eq. (6) is replaced with integration, the Skellam distribution (7) can be approximated assuming that the amplitude of the local oscillator, $|\alpha_L|$, is large (the strong LO approximation) and we can apply the convolution formula for Gaussian probability densities

$$\int G(x_1 - x_2; \sigma_1)G(x_2; \sigma_2)\mathrm{d}x_2 = G(x_1; \sigma_1 + \sigma_2), \quad (8)$$

$$G(x; \sigma) \equiv \frac{1}{\sqrt{2\pi\sigma}} \exp\left(-\frac{x^2}{2\sigma}\right). \quad (9)$$

The above procedure immediately leads to the Gaussian approximation of the form:

$$\mathsf{P}_G(\mu) = G(\mu - \mu_G; \sigma_G), \quad (10)$$

$$\sigma_G = \eta_1|\alpha_1|^2 + \eta_2|\alpha_2|^2 \approx (\eta_1 S^2 + \eta_2 C^2)|\alpha_L|^2, \quad (11)$$

$$\mu_G = \eta_1|\alpha_1|^2 - \eta_2|\alpha_2|^2 \approx (\eta_1 S^2 - \eta_2 C^2)|\alpha_L|^2$$
$$+ CS(\eta_1 + \eta_2)|\alpha_L|\langle\hat{x}_\phi\rangle \quad (12)$$

where

$$\langle\hat{x}_\phi\rangle \equiv \langle\alpha|\hat{x}_\phi|\alpha\rangle = 2\,\mathrm{Re}\,\alpha e^{-i\phi}, \quad \phi = \arg\alpha_L \quad (13)$$

is the average of the phase-rotated quadrature operator of the signal mode given by

$$\hat{x}_\phi = \hat{a}e^{-i\phi} + \hat{a}^\dagger e^{i\phi}. \quad (14)$$

Alternatively, the probability (10) can be rewritten in the form

$$\mathsf{P}_G(x) = \frac{1}{\sqrt{2\pi\sigma_G}} \exp\left\{-\frac{(x - \langle\hat{x}_\phi\rangle)^2}{2\sigma_x}\right\}, \quad (15)$$

where x is the quadrature variable given by

$$x \equiv \frac{\mu}{(\eta_1 + \eta_2)CS|\alpha_L|} - \frac{\eta_1 S^2 - \eta_2 C^2}{(\eta_1 + \eta_2)\,CS}|\alpha_L| \quad (16)$$

and σ_x is the quadrature variance

$$\sigma_x \equiv \frac{\eta_1 S^2 + \eta_2 C^2}{[(\eta_1 + \eta_2)CS]^2}. \quad (17)$$

Note that it is rather straightforward to minimize the variance (17) with respect to the transmittance, C^2, and deduce inequality

$$\sigma_x \geq \sigma_x^{(\mathrm{min})} = \left(\frac{\sqrt{\eta_1} + \sqrt{\eta_2}}{\eta_1 + \eta_2}\right)^2 \geq 1, \quad (18)$$

where σ_x reaches its minimum value $\sigma_x^{(\mathrm{min})}$ at the beam splitter transmittance: $C^2 = \cos^2\theta_{\mathrm{min}} = \sqrt{\eta_1}/(\sqrt{\eta_1} + \sqrt{\eta_2})$.

Our next step is to construct the positive operator-valued measure (POVM) based on the Gaussian approximation P_G. To this end, note that the probability (15) is the expectation value of the POVM in the coherent state given by

$$\mathsf{P}_G = \langle\alpha|\hat{\Pi}_G|\alpha\rangle. \quad (19)$$

In the case of the perfectly symmetric homodyne measurement with $\eta_1 = \eta_2 = 1$ and $C = S = 1/\sqrt{2}$, the average (19) takes the form

$$\mathsf{P}_G^{(0)} = \frac{1}{|\alpha_L|}Q_{x,\phi}(\alpha), \quad (20)$$

where $x = \mu/|\alpha_L|$ and $Q_{x,\phi}(\alpha)$ is the Husimi Q distribution for the eigenstate of the phase-rotated quadrature operator (14), $|x, \phi\rangle$, given by (see, e.g., the textbook[30])

$$Q_{x,\phi}(\alpha) = |\langle\alpha|x, \phi\rangle|^2 = G(x - \langle\hat{x}\rangle_\phi; 1). \quad (21)$$

Thus, we are led to the well-known result that POVM describing sharp homodyne measurements in the Gaussian approximation is proportional to a projector onto $|x, \phi\rangle$:

$$\hat{\Pi}_G^{(0)} = \frac{1}{|\alpha_L|}|x, \phi\rangle\langle x, \phi|, \quad (22)$$

In a more general asymmetric case with $\eta_1 \neq \eta_2$ and $C \neq S$, the Gaussian-shaped probability P_G can be represented as a Gaussian superposition written as a convolution of $P_G^{(0)}$ and a Gaussian function $G(x, \sigma_N)$. By using the convolution identity (8), we have

$$\mathsf{P}_G(x) = \sqrt{\frac{\sigma_x}{\sigma_G}} \int G(x - x'; \sigma_N)\mathsf{P}_G^{(0)}(x')\mathrm{d}x', \quad (23)$$

$$\sigma_N = \sigma_x - 1 \geq 0, \quad (24)$$

where non-negativity of the variance σ_N stems from Eq. (18). This result immediately gives a general formula for the Gaussian approximation POVM

$$\hat{\Pi}_G = \frac{1}{(\eta_1 + \eta_2)CS|\alpha_L|}$$
$$\times \int \mathrm{d}x' G(x - x'; \sigma_N)|x', \phi\rangle\langle x', \phi|. \quad (25)$$

Note that the variance σ_N describes the excess noise that takes into account asymmetry effects.

In the limiting case of perfect homodyne, we have

$$\lim_{\sigma_x \to 1} G(x; \sigma_N) = \lim_{\sigma_N \to 0} G(x; \sigma_N) = \delta(x), \quad (26)$$

where $\delta(x)$ is the Dirac δ-function, which is the expected behavior for Eq. (23) to hold . Therefore, the constructed POVM (25) is well-defined for all possible parameters of the homodyne scheme.

Our concluding remark concerns an alternative method to approximate Eq. (7) with a Gaussian-shaped distribution which is based on the asymptotic expansions of the modified Bessel functions. In Appendix A we show that, for the asymmetric homodyne scheme, this method generally leads to ill-posed POVMs because the corresponding quadrature variance appears to be too small leading to negative contribution of the excess noise.
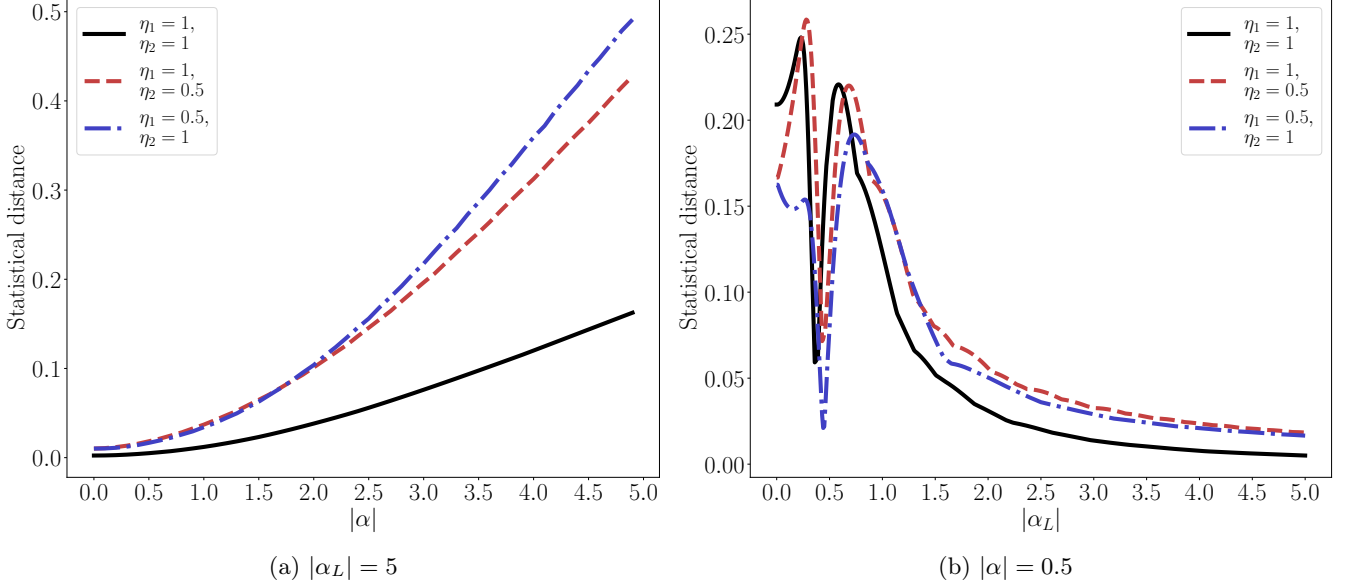
(a) $|\alpha_L| = 5$

(b) $|\alpha| = 0.5$

Figure 2: Statistical distance $D_P = \mathsf{D}(\mathsf{P}, \mathsf{P}_G)$ as a function of (a) signal amplitude and (b) LO amplitude at different detector efficiencies.

B. Numerical results

In this section, we begin with the case where the signal mode is in the coherent state $|\alpha\rangle$ and compare the exact statistics of difference events governed by the Skellam distribution (7) and the Gaussian approximation (10). In order to quantify the statistical distance between the probability distributions, we shall use the total variational distance that can be computed as half of the L^1 distance

$$D_P \equiv \mathsf{D}(\mathsf{P}, \mathsf{P}_G) \equiv \frac{1}{2} \sum_{\mu=-\infty}^{\infty} |\mathsf{P}(\mu) - \mathsf{P}_G(\mu)|. \qquad (27)$$

Note that, according to Eq. (27), μ takes integer values and we evaluate the distance between the probability mass fuctions, whereas the normalization condition for the Gaussian function (10)

$$\int_{-\infty}^{\infty} \mathsf{P}_G(\mu)\mathrm{d}\mu = 1 \qquad (28)$$

implies applicability of the continuum limit. For integer μ, the integral on the left hand side of Eq. (28) should be replaced with a sum and we have the relation

$$\sum_{\mu=-\infty}^{\infty} \mathsf{P}_G(\mu) = \vartheta_3(\pi\mu_G, e^{-2\pi^2\sigma_G}) \equiv N_G \qquad (29)$$

where ϑ_3 is the Jacobi elliptic theta function [29].

In the applicability region of the continuum limit, the normalization constant N_G is close to unity. The numerical analysis shows that $|N_G - 1| \leq 10^{-4}$ at $2\sigma_G \geq 1$.

The latter gives the condition for the LO amplitude

$$|\alpha_L| \geq \frac{1}{\sqrt{2(\eta_1 S^2 + \eta_2 C^2)}} \equiv \alpha_N \qquad (30)$$

which ensures both applicability of the continuum limit and proper normalization of the Gaussian approximation. In our calculations, the probability P_G will be numerically corrected by introducing the factor N_G^{-1} provided that $|\alpha_L|$ is below the "renormalization point" α_N.

The curves presented in Fig. 2 illustrate how the accuracy of the Gaussian approximation is affected by the signal and LO amplitudes, $|\alpha|$ and $|\alpha_L|$. More specifically, in Fig. 2a (Fig. 2b), the statistical distance is numerically evaluated as a function of the amplitude $|\alpha|$ ($|\alpha_L|$) at different values of the photodetectors efficiencies provided that the value of the other amplitude $|\alpha_L|$ ($|\alpha|$) is fixed.

Referring to Fig. 2a, the curves behave as expected: given the LO amplitude $|\alpha_L|$, the distance monotonically increases with $|\alpha|$. It is shown that, at $|\alpha_L| = 5$ and $|\alpha| > 1$, the perfectly symmetric homodyne presents the case with minimal distance, D_P, while in the presence of asymmetry, the curves exhibit a rapid growth and the quality of the Gaussian approximation rapidly degrades to the point, where $D_P > 0.1$, so it is not useful for its intended purpose.

When it comes to dependencies of the statistical distance on the LO oscillator amplitude computed at fixed value of $|\alpha|$, the above results suggest that the smaller the amplitude $|\alpha|$ the better the accuracy of the Gaussian approximation. We can also expect the distance will be small provided that $|\alpha_L|$ is large and the strong LO approximation is applicable.

Referring to Fig. 2b, the curves evaluated at $|\alpha| = 0.5$ display a non-monotonic behavior with two local maxima
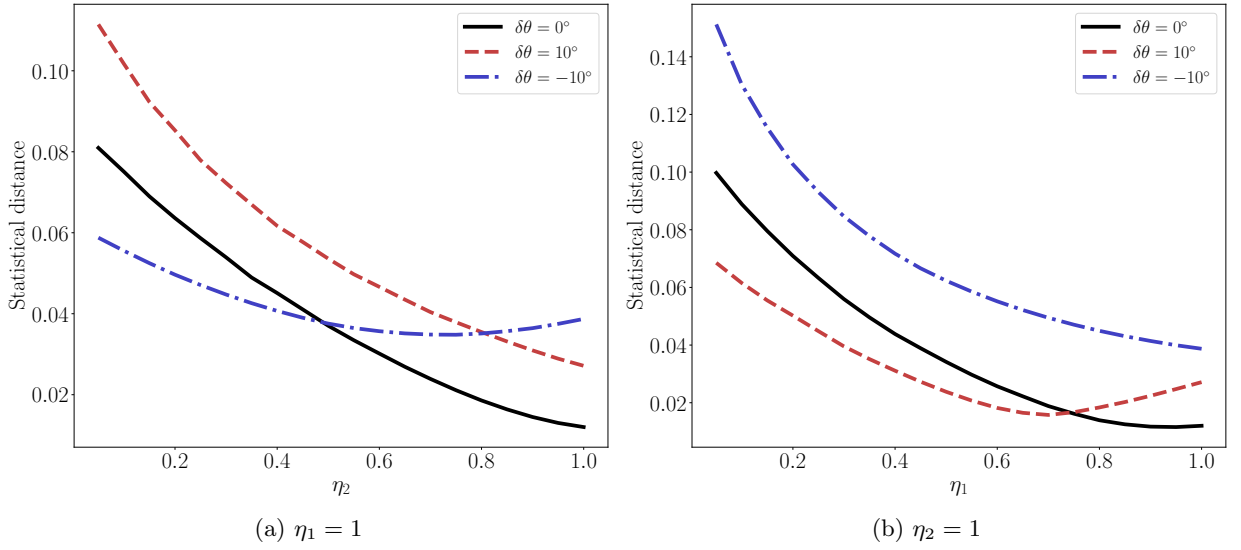
Figure 3: Statistical distance $D_P = \mathrm{D}(\mathsf{P}, \mathsf{P}_G)$ as a function of photodetector efficiency (a) η_2 at $\eta_1 = 1$ and (b) η_1 at $\eta_2 = 1$ for different values of the beam splitter disbalance angle $\delta\theta$ (see eq. (31)). The amplitudes are $|\alpha| = 1$ and $|\alpha_L| = 5$.
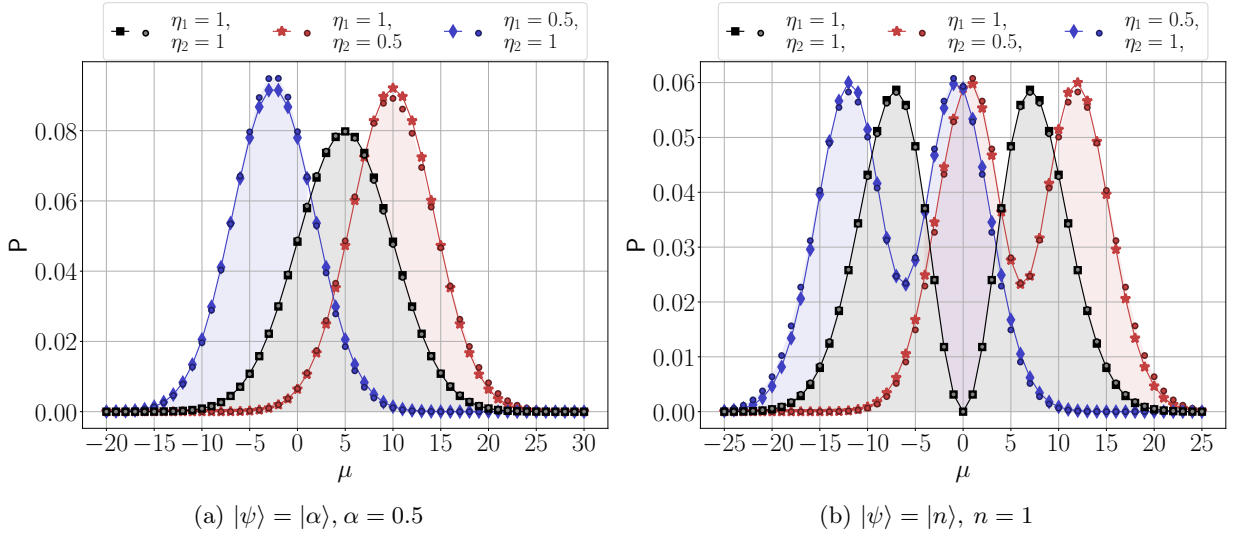

Figure 4: Statistical distributions of photon count difference for the signal mode prepared in (a) the coherent state and in (b) the single photon Fock state computed for for different efficiencies at $|\alpha_L| = 5$ and $\delta\theta = 0$.

in the weak LO range where $|\alpha_L| < 1$. By contrast, after the second maximum at $|\alpha_L| > 1$, the distance falls with the LO amplitude and it drops below 0.05 at $|\alpha_L| > 2$.

Note, that, when $|\alpha| < 0.1$ and the signal mode state is close to the vacuum state, the two local maxima of D_P can be estimated to be slightly above 0.08 and 0.1, respectively. So, in this case, the distribution (10) might be regarded as a reasonable approximation even in the weak LO range where the probability P_G approaches the close neighborhood of the singular limit, $\lim_{|\alpha_L| \to 0} \mathsf{P}_G(\mu) = \delta(\mu)$.

From Fig. 2b, it can also be seen that the distance vs

LO amplitude dependence that can be used as a tool to characterize the applicability region of the strong LO approximation is nearly insensitive to asymmetry. In other words, the latter does not produce noticeable effects on the accuracy of the approximation.

The parameters describing the photodetection asymmetry are the efficiencies η_1 and η_2. The curves plotted in Fig. 2 are computed at different values of the efficiencies.

In order to quantify deviation of the beam splitter transmission and reflection amplitudes from the balanced $50 : 50$ values $t = \cos\theta = r = \sin\theta = 1/\sqrt{2}$ at the angle
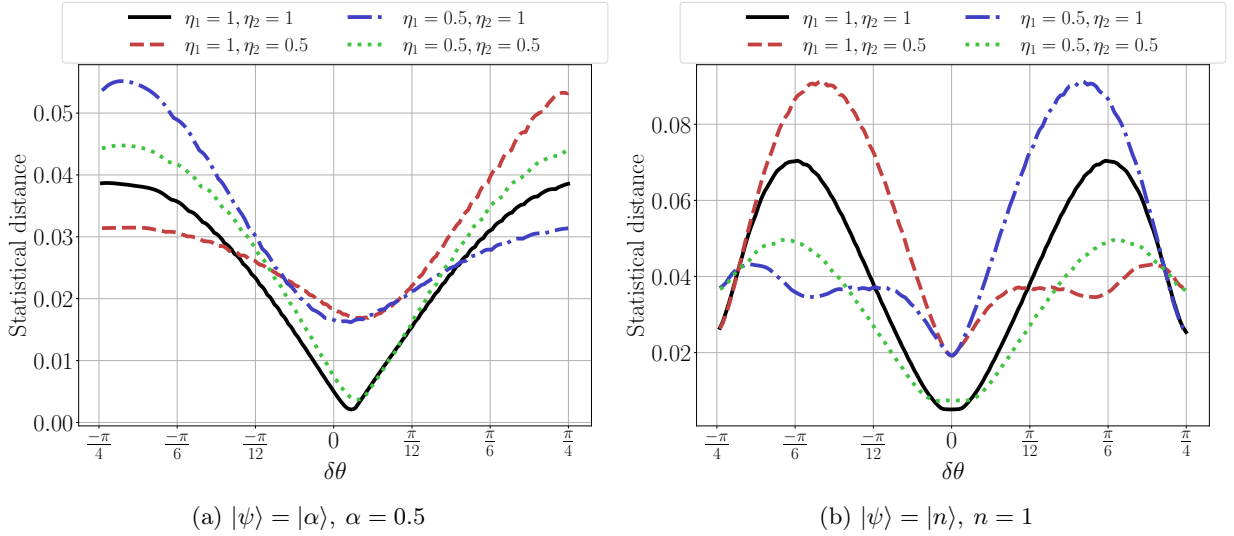
(a) $|\psi\rangle = |\alpha\rangle$, $\alpha = 0.5$

(b) $|\psi\rangle = |n\rangle$, $n = 1$

Figure 5: Statistical distance $D_P = \mathsf{D}(\mathsf{P}, \mathsf{P}_G)$ as a function of the beam splitter disbalance angle, $\delta\theta$, for the signal mode prepared in (a) the coherent state and in (b) the single photon Fock state at different efficiencies with $|\alpha_L| = 5$.

$\theta = \pi/4$, we introduce the beam splitter *disbalance angle* given by

$$\delta\theta \equiv \frac{\pi}{4} - \theta. \qquad (31)$$

In Figure 3 we plot the distance against the efficiency of the photodetector assuming that the other photodetector is perfect. The curves are evaluated at different values of the disbalance angle (31). The efficiency dependence of the distance is shown to decrease monotonically at $\delta\theta = 0$. In contrast, for disbalanced beam splitter, this dependence can reveal non-motonic behavior.

So far, we have used the analytical results obtained in Sec. II A for the case where the LO and signal modes are both in the coherent states. In the general case when the quantum state of the signal mode is $|\psi\rangle$, the probability distributions can be evaluated using the relations

$$\mathsf{P}(\mu; |\psi\rangle) = \int P_{|\psi\rangle}(\alpha)\mathsf{P}(\mu; \alpha)\mathrm{d}^2\alpha,$$
$$\mathsf{P}_G(x; |\psi\rangle) = \langle\psi|\hat{\Pi}_G|\psi\rangle, \qquad (32)$$

where $P_{|\psi\rangle}(\alpha)$ is the Glauber P function of the quantum state $|\psi\rangle$. In Figs. 4 and 5, we show the results computed for the single-photon Fock states obtained utilizing the well-known expression for the P-function of Fock states $|\psi\rangle = |n\rangle$ given by

$$P_{|n\rangle}(\alpha) = \frac{e^{|\alpha|^2}}{n!}\left(\frac{\partial^2}{\partial\alpha\partial\alpha^*}\right)^n\delta^2(\alpha), \qquad (33)$$

where $\delta^2(\alpha) = \delta(\mathrm{Re}\,\alpha)\delta(\mathrm{Im}\,\alpha)$.

Figure 4 displays the photocount difference probabilities computed from the exact and Gaussian probability distributions for the balanced beam splitter at different photodetector efficiencies and signal mode input

states. From Fig. 4a, it is seen that, in agreement with Eq. (12), asymmetry in photodetection results in the shift of the probability maximum. Note that, at $\delta\theta = 0$, the photocount variance (11), $\sigma_G = (\eta_1 + \eta_2)|\alpha_L|^2/2$, and the quadrature variance (17), $\sigma_x = 2/(\eta_1 + \eta_2)$, are both invariant under transposition of the photodetectors: $\eta_1 \leftrightarrow \eta_2$.

The distributions for the single-photon states are depicted in Fig. 4b and, similar to the coherent state, demonstrate the effect of asymmetry-induced shift. Another noticeable effect is that the probability minima between the central and side peaks become less pronounced.

The photodetector efficiencies and the signal mode input states of Fig. 4 are used to compute the statistical distance vs disbalance angle curves presented in Fig. 5. These curves illustrate how the beam splitter disbalance and the photodetector efficiencies influence the accuracy of the Gaussian approximation. The distance is shown to be minimal in the vicinity of the balanced beam splitter point with a vanishing disbalance angle, $\delta\theta = 0$.

III. DOUBLE HOMODYNE DETECTION

In the section, we consider the eight-port double homodyne scheme depicted in Fig. 6 (see, e.g., Refs. [30, 31]). This measurement scheme is known to allow reconstructing the Husimi Q function of the signal state [32] providing complete information about the signal state that may be used in CV-QKD protocols. It should be noted that restoration of the complex amplitude of the state completely serves as the basis for composable security proofs [2, 33].

Figure 6 shows two homodyne setups with elements such as beam splitters BS_i and photodetectors $D_{1,2}^{(i)}$ la-
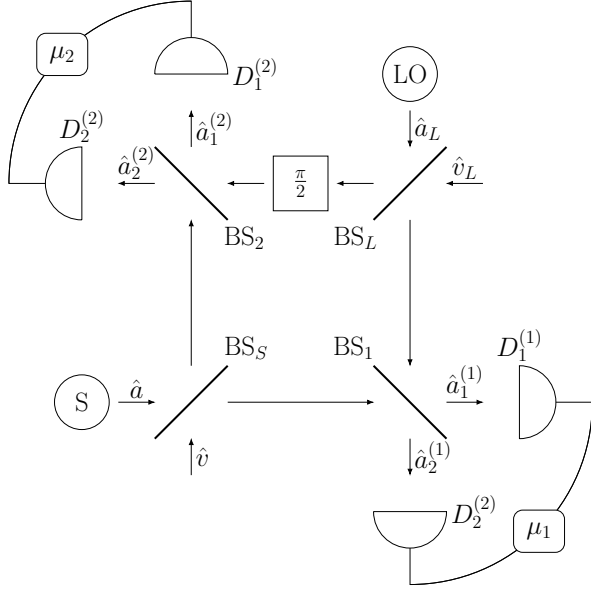
Figure 6: Scheme of an eight port double homodyne receiver. S is the source of the signal mode $\hat{a}$; LO is the source of the reference mode $\hat{a}_L$; BS_S (BS_L) is the signal mode (local oscillator) beam splitter; $\frac{\pi}{2}$ is the quarter wave phase shifter; BS_i is the beam splitter of ith homodyne; $D_{1,2}^{(i)}$ are the photodetectors of the ith homodyne; and $\mu_i = m_1^{(i)} - m_2^{(i)}$ is the photon count difference registered by the detectors of ith homodyne.

beled by the index $i \in \{1, 2\}$. Referring to Fig. 6, the LO and signal modes are transmitted through the beam splitters BS_L and BS_S, respectively. Similar to the analysis performed in the previous section, we assume that the modes are in the coherent states, $|\alpha\rangle$ and $|\alpha_L\rangle$. So, we have the amplitudes

$$\alpha^{(1)} = C_S \alpha, \quad \alpha^{(2)} = S_S \alpha,$$
$$\alpha_L^{(1)} = C_L \alpha_L, \quad \alpha_L^{(2)} = -i S_L \alpha_L, \quad (34)$$

where $\alpha^{(i)}$ ($\alpha_L^{(i)}$) stands for the amplitude describing the input coherent state of the signal (LO) mode of the homodyne labeled by the upper index $i \in \{1, 2\}$. Note that the phase factor $-i = e^{-i\pi/2}$ in the expression for $\alpha_L^{(2)}$ is introduced by a suitably chosen phase shifter placed before the corresponding input port of the beam splitter BS_2.

It is rather straightforward to see that the joint statistics of the difference photocount events is determined by the product of the Skellam distributions given by

$$P(\mu_1, \mu_2) = P_1(\mu_1) P_2(\mu_2), \quad \mu_i = m_1^{(i)} - m_2^{(i)}, \quad (35)$$

$$P_i(\mu_i) = e^{-\eta_1^{(i)}|\alpha_1^{(i)}|^2} e^{-\eta_2^{(i)}|\alpha_2^{(i)}|^2} \left(\frac{\eta_1^{(i)}|\alpha_1^{(i)}|^2}{\eta_2^{(i)}|\alpha_2^{(i)}|^2} \right)^{\mu_i/2}$$
$$\times I_{\mu_i}\big(2\sqrt{\eta_1^{(i)} \eta_2^{(i)} |\alpha_1^{(i)}|^2 |\alpha_2^{(i)}|^2} \big), \quad (36)$$

where, similar to the homodyne scheme, the amplitudes of the coherent states at the output ports of the beam splitter BS_i

$$\alpha_1^{(i)} = C_i \alpha^{(i)} + S_i \alpha_L^{(i)}, \quad \alpha_2^{(i)} = -S_i \alpha^{(i)} + C_i \alpha_L^{(i)} \quad (37)$$

are expressed in terms of the transmission and reflection amplitudes, $C_i = \cos \theta_i$ and $S_i = \sin \theta_i$.

We can now apply Eqs. (10)–(12) to approximate each Skellam distribution on the right hand side of Eq. (35) and derive the Gaussian approximation for the double homodyne scheme in the form:

$$P_G(\mu_1, \mu_2) = G(\mu_1 - \mu_G^{(1)}; \sigma_G^{(1)}) G(\mu_2 - \mu_G^{(2)}; \sigma_G^{(2)}), \quad (38)$$

$$\sigma_G^{(i)} = (\eta_1^{(i)} S_i^2 + \eta_2^{(i)} C_i^2)|\alpha_L^{(i)}|^2, \quad (39)$$

$$\mu_G^{(i)} = (\eta_1^{(i)} S_i^2 - \eta_2^{(i)} C_i^2)|\alpha_L^{(i)}|^2 + C_i S_i (\eta_1^{(i)} + \eta_2^{(i)})|\alpha_L^{(i)}|$$
$$\times 2 \operatorname{Re} \alpha^{(i)} e^{-i\phi}, \quad \phi = \arg \alpha_L. \quad (40)$$

Similar to Eq. (15), it is useful to put the probability (38) into the folowing quadrature form:

$$P_G(x_1, x_2) = \frac{1}{2\pi\sqrt{\sigma_G^{(1)} \sigma_G^{(2)}}} \exp\left\{ -\frac{(x_1 - \operatorname{Re} \alpha e^{-i\phi})^2}{\sigma_1} \right.$$
$$\left. - \frac{(x_2 - \operatorname{Im} \alpha e^{-i\phi})^2}{\sigma_2} \right\} \quad (41)$$

where x_i are the quadrature variables given by

$$x_1 = \frac{1}{2(\eta_1^{(1)} + \eta_2^{(1)}) C_1 S_1 C_S}$$
$$\times \left\{ \frac{\mu_1}{|\alpha_L^{(1)}|} - (\eta_1^{(1)} S_1^2 - \eta_2^{(1)} C_1^2)|\alpha_L^{(1)}| \right\}, \quad (42)$$

$$x_2 = \frac{1}{2(\eta_1^{(2)} + \eta_2^{(2)}) C_2 S_2 S_S}$$
$$\times \left\{ \frac{\mu_2}{|\alpha_L^{(2)}|} - (\eta_1^{(2)} S_2^2 - \eta_2^{(2)} C_2^2)|\alpha_L^{(2)}| \right\}, \quad (43)$$

and relations

$$\sigma_1 = \frac{\sigma_x^{(1)}}{2C_S^2}, \quad \sigma_2 = \frac{\sigma_x^{(2)}}{2S_S^2}, \quad (44)$$

$$\sigma_x^{(i)} = \frac{\eta_1^{(i)} S_i^2 + \eta_2^{(i)} C_i^2}{\left[(\eta_1^{(i)} + \eta_2^{(i)}) C_i S_i \right]^2} \quad (45)$$

give the quadrature variances σ_1 and σ_2.

As in Sec. II A, formula (41) giving the Q-symbol of POVM (see Eq. (19)) provides the starting point for reconstruction of the POVM describing the double homodyne measurements. In the ideal case, where all the beam splitters are balanced and the photodetection is perfect, we have

$$P_G^{(0)}(x_1, x_2) = \frac{|\langle z|\alpha\rangle|^2}{\pi|\alpha_L|^2}, \quad |\langle z|\alpha\rangle|^2 = e^{-|z-\alpha|^2}, \quad (46)$$

(a) $\eta_1^{(i)} = 1, \eta_2^{(i)} = 1$ (b) $\eta_1^{(i)} = 1, \eta_2^{(i)} = 0.5$ (c) $\eta_1^{(i)} = 1, \eta_2^{(1)} = 1, \eta_2^{(2)} = 0.5$
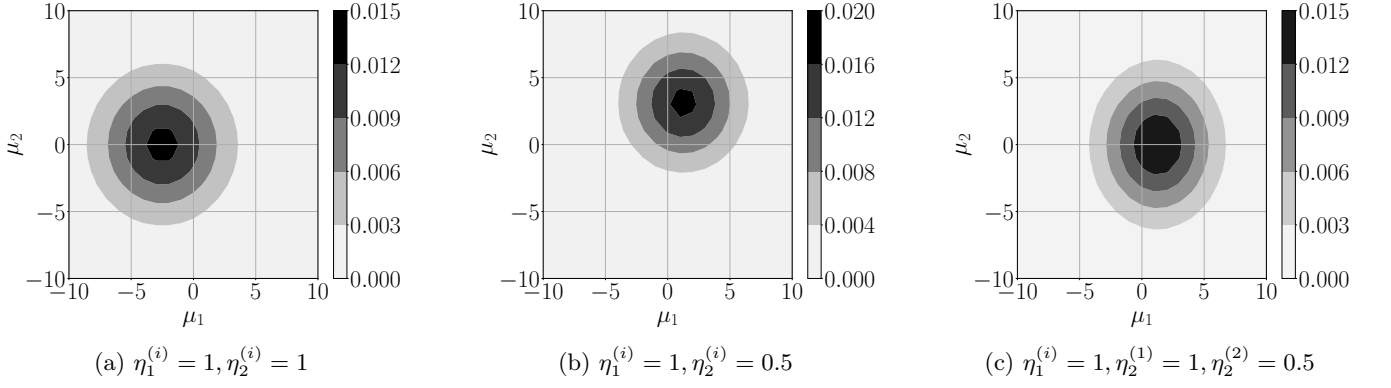
Figure 7: Double homodyne statistical distribution of photocount differences computed from Eq. (35) for various detector efficiencies at $\alpha = 0.5$ and $\alpha_L = 5$. All the beam splitters are taken to be balanced.

where

$$z = (x_1 + ix_2)e^{i\phi}, \quad x_i = \frac{\mu_i}{|\alpha_L|}. \tag{47}$$

So, the POVM is proportional to a projector onto the coherent state $|z\rangle \equiv |(x_1 + ix_2)e^{i\phi}\rangle$:

$$\hat{\Pi}_G^{(0)}(x_1, x_2) = \frac{1}{\pi|\alpha_L|^2}|z\rangle\langle z|. \tag{48}$$

For non-ideal measurements, the probability (41) can be expressed as a Gaussian superposition of the coherent state Husimi functions with the help of the convolution relation (8) as follows

$$\mathsf{P}_G(x_1, x_2) = \frac{\sqrt{\sigma_1 \sigma_2}}{2\pi\sqrt{\sigma_G^{(1)}\sigma_G^{(2)}}} \int d\beta_1 d\beta_2 G(x_1 - \beta_1; \sigma_N^{(1)})$$

$$\times G(x_2 - \beta_2; \sigma_N^{(2)})|\langle\beta e^{i\phi}|\alpha\rangle|^2, \quad \beta = \beta_1 + i\beta_2, \tag{49}$$

where the excess noise variance $\sigma_N^{(i)}$ is determined by the relation

$$2\sigma_N^{(i)} = \sigma_i - 1. \tag{50}$$

The corresponding expression for the POVM reads

$$\hat{\Pi}_G(x_1, x_2) = \frac{\sqrt{\sigma_1 \sigma_2}}{2\pi\sqrt{\sigma_G^{(1)}\sigma_G^{(2)}}} \int d\beta_1 d\beta_2 G(x_1 - \beta_1; \sigma_N^{(1)})$$

$$\times G(x_2 - \beta_2; \sigma_N^{(2)})|\beta e^{i\phi}\rangle\langle\beta e^{i\phi}|. \tag{51}$$

An important point is that the results given by Eq. (49) and Eq. (51) are well defined only if σ_1 and σ_2 are both above unity, so that the excess noise variances (50) are positive. From Eq. (44), this requires that conditions $\sigma_x^{(1)} \geq 2C_S^2$ and $\sigma_x^{(2)} \geq 2S_S^2$ be met.

When the beam splitter BS_S is balanced $2C_S^2 = 2S_S^2 = 1$ and inequality (see Eq. (18))

$$\sigma_x^{(i)} \geq \left(\frac{\sqrt{\eta_1^{(i)}} + \sqrt{\eta_2^{(i)}}}{\eta_1^{(i)} + \eta_2^{(i)}}\right)^2 \geq 1 \tag{52}$$

ensures applicability of the expression for the POVM. Otherwise, either $2C_S^2$ or $2S_S^2$ will be above unity, and our results are valid only if the value of the corresponding variance $\sigma_x^{(i)}$ is sufficiently high. For example, at $\eta_{1,2}^{(i)} = \eta < 1/2$, the minimal values of $\sigma_x^{(i)}$ are higher than 2 (see Eq. (52)) and the noise variance will be positive at any disbalance of the signal mode beam splitter because $\max\{2C_S^2, 2S_S^2\} \leq 2$. When the noise variance is negative, the POVM reconstruction procedure needs to be generalized. We shall present details on this generalization in the next section. Meanwhile, in the remaining part of this section, we confine ourselves to the cases where $\sigma_N^{(i)}$ are positive.

The effects of photodetection asymmetry are illustrated in Fig. 7 which presents numerical results for the double homodyne distribution (35) in the photocont difference μ_1-μ_2 plane. Referring to Fig. 7, in addition to the shift of the distribution, the asymmetry induced difference of the variances at $\eta_1^{(1)} + \eta_2^{(1)} \neq \eta_1^{(2)} + \eta_1^{(2)}$ manifests itself as the two dimensional anisotropy of the double homodyne distribution.

IV. POSITIVE OPERATOR-VALUED MEASURE AND SQUEEZED STATES

From Eq. (50), the expression for the POVM in the form of incoherent gaussian superposition of coherent states is justified only if both the quadrature variances, σ_1 and σ_2, exceed unity. In this section, we show that our procedure employed for derivation of the double homodyne POVM can be suitably generalized by enlarging a set of the pure states to include the squeezed coherent states

$$|\beta, \xi\rangle = \hat{D}(\beta)\hat{S}(\xi)|0\rangle, \tag{53}$$

where $\hat{D}(\beta)$ ($\hat{S}(\xi)$) is the displacement (squeezing) operator given by

$$\hat{D}(\beta) = e^{\beta\hat{a}^\dagger - \beta^*\hat{a}}, \quad \hat{S}(\xi) = e^{\frac{1}{2}(\xi\hat{a}^{\dagger 2} - \xi^*\hat{a}^2)}, \tag{54}$$

β and ξ are the complex-valued amplitude and the squeeze parameter, respectively.

To this end, we consider the case, where the squeeze parameter is given by

$$\xi = re^{2i\phi}, \quad r \in \mathbb{R} \tag{55}$$

and the non-normalized Husimi distribution for the squeezed state (53) takes the form (see, e.g., the textbook [34])

$$|\langle \beta, re^{2i\phi}|\alpha\rangle|^2 = \frac{1}{\cosh r} \exp\left\{ -\frac{e^{-r}}{\cosh r} \left(\tilde{\beta}_1 e^r - \tilde{\alpha}_1 \right)^2 \right.$$
$$\left. - \frac{e^r}{\cosh r} \left(\tilde{\beta}_2 e^{-r} - \tilde{\alpha}_2 \right)^2 \right\}, \tag{56}$$
$$\tilde{\beta} = \tilde{\beta}_1 + i\tilde{\beta}_2 = \beta e^{-i\phi}, \quad \tilde{\alpha} = \tilde{\alpha}_1 + i\tilde{\alpha}_2 = \alpha e^{-i\phi}. \tag{57}$$

By using this squeezed state distribution instead of the coherent state one given in Eq. (48), we are led to the expressions for the noise variances modified as follows

$$2\sigma_N^{(1,2)} = \sigma_{1,2} - e^{\pm r} \cosh r. \tag{58}$$

These expressions present the extension of the relations (50) to the case with non-vanishing squeeze parameter. As an immediate consequence of Eq. (58), we find that the conditions for the noise variances to be positive definite can be written in the form of two inequalities

$$4\sigma_N^{(1)} = \delta_1 - e^{2r} \geq 0, \quad 4\sigma_N^{(2)} = \delta_2 - e^{-2r} \geq 0, \tag{59}$$

where the quadrature variance parameters

$$\delta_1 = 2\sigma_1 - 1 = (q+1)\sigma_x^{(1)} - 1 \geq q = \frac{S_S^2}{C_S^2}, \tag{60a}$$

$$\delta_2 = 2\sigma_2 - 1 = (q^{-1}+1)\sigma_x^{(2)} - 1 \geq q^{-1} = \frac{C_S^2}{S_S^2} \tag{60b}$$

are expressed in terms of the disbalance (reflection-to-transmission) ratio of the input beam splitter, q, and the parameters $\sigma_x^{(1)}$ and $\sigma_x^{(2)}$ (see Eq. (45)) that cannot be smaller than unity (see Eq. (52)): $\sigma_x^{(i)} \geq 1$.

In our subsequent analysis, we assume without the loss of generality that the reflectance of the input beam splitter BS_S is larger than its transmittance, so that the disbalance ratio is above unity

$$q = \frac{1 - C_S^2}{C_S^2} = \frac{S_S^2}{C_S^2} \geq 1. \tag{61}$$

As is shown in Fig. 8, this implies that the variance δ_1 is above unity: $\delta_1 \geq q \geq 1$, whereas the minimal value of δ_2 is $q^{-1} \leq 1$. It is illustrated that the noise variances are positive provided the squeeze parameter r is ranged between the endpoints of the interval given by

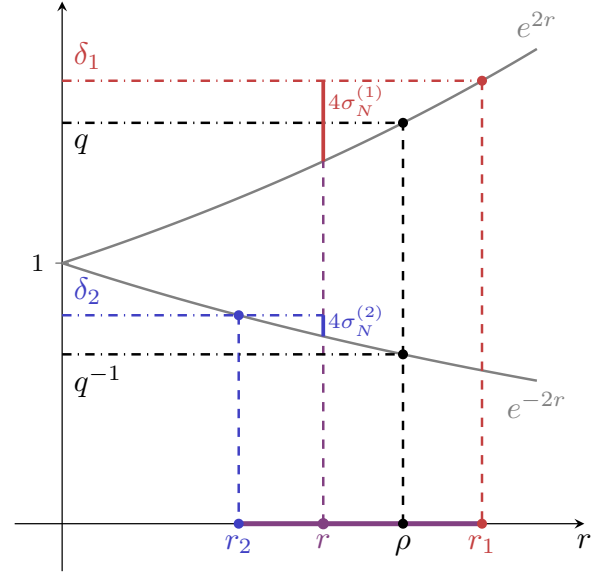$$r \in [r_2, r_1], \; r_1 = \ln \delta_1^{1/2}, \; r_2 = \max\{\ln \delta_2^{-1/2}, 0\}. \tag{62}$$

Figure 8: An illustration for the conditions for the noise variances, see Eqs. (59)-(62). Solid grey lines represent the exponents $e^{\pm 2r}$. Dashdotted black, red and blue lines are the independent on r functions q and q^{-1}, δ_1 and δ_2 respectively. Solid purple line is the interval of squeezing parameter $r \in [r_2, r_1]$, solid red (blue) line is the magnitude of $4\sigma_N^{(1)}$ ($4\sigma_N^{(2)}$) at r.

An important point is that the value of the squeeze parameter is not uniquely determined by the conditions (59). We have a unique value of the squeeze parameter only in the limiting case of perfect homodyne measurements with $\sigma_x^{(1)} = \sigma_x^{(2)} = 1$ and $\delta_1 = \delta_2^{-1} = q$. In this case, the squeeze parameter is unambiguously defined

$$r_1 = r_2 = \rho = \frac{1}{2} \ln q = \ln \sqrt{\frac{1 - C_S^2}{C_S^2}} \tag{63}$$

and the probability (41) expressed in terms of the distribution (56)

$$\mathsf{P}_G^{(1)}(x_1, x_2) = \frac{\cosh \rho}{2\pi |\alpha_L^{(1)} \alpha_L^{(2)}|} |\langle \beta e^{i\phi}, \rho e^{2i\phi}|\alpha\rangle|^2, \tag{64}$$

$$\beta = e^{-\rho} x_1 + i e^{\rho} x_2 \tag{65}$$

yields the POVM

$$\hat{\Pi}_G^{(1)}(x_1, x_2) = \frac{\cosh \rho}{2\pi |\alpha_L^{(1)} \alpha_L^{(2)}|}$$
$$\times |\beta e^{i\phi}, \rho e^{2i\phi}\rangle\langle \beta e^{i\phi}, \rho e^{2i\phi}|, \tag{66}$$

which is propotional to the pure squeezed state $|\beta e^{i\phi}, \rho e^{2i\phi}\rangle$. The result (63) was reported in Ref. [35].

When the homodyne measurements are not perfect due to unbalanced beam splitters and nonideal photodetectors, the squeeze parameter is no longer uniquely defined.

So, in the interval (62), we have the decomposition of the probability (41)

$$
\begin{aligned}
\mathsf{P}_G(x_1, x_2) = {} & \frac{\sqrt{\sigma_1 \sigma_2}}{2\pi \sqrt{\sigma_G^{(1)} \sigma_G^{(2)}}} \\
& \times \int \mathrm{d}\beta_1 \mathrm{d}\beta_2 \, G(x_1 e^{-r} - \beta_1; \sigma_N^{(1)}(r) e^{-2r}) \\
& \times G(x_2 e^r - \beta_2; \sigma_N^{(2)}(r) e^{2r}) |\langle \beta e^{i\phi}, r e^{2i\phi} | \alpha \rangle|^2
\end{aligned}
\tag{67}
$$

that varies with the squeeze parameter r. Similarly, the corresponding POVM

$$
\begin{aligned}
\hat{\Pi}_G(x_1, x_2) = {} & \frac{\sqrt{\sigma_1 \sigma_2}}{2\pi \sqrt{\sigma_G^{(1)} \sigma_G^{(2)}}} \\
& \times \int \mathrm{d}\beta_1 \mathrm{d}\beta_2 \, G(x_1 e^{-r} - \beta_1; \sigma_N^{(1)}(r) e^{-2r}) \\
& \times G(x_2 e^r - \beta_2; \sigma_N^{(2)}(r) e^{2r}) \\
& \times |\beta e^{i\phi}, r e^{2i\phi}\rangle\langle \beta e^{i\phi}, r e^{2i\phi}|
\end{aligned}
\tag{68}
$$

decomposed into the Gaussian incoherent superposition of the pure squeezed states explicitly depends on the value of r. Our analysis suggests that the ambiguity (non-uniqueness) of the Gaussian representation (68) for the double-homodyne POVM is a universal feature coming into play in the presence of imperfections. Even when $\delta_2 \geq 1$ and the coherent-state representation (51) for the POVM is well-defined, the photocount statistics can be reproduced using the squeezed-state representation (68) with $0 < r \leq r_1$. One of the way to make the Gaussian POVM decomposition unique is to place additiona constraints on the noise variances that would fix the value of the squeeze parameter. For example, the squeeze parameter would take the minimal (maximal) value: $r = \min\{r_1, r_2\}$ ($r = \max\{r_1, r_2\}$) provided the constraint requires minimization of the noise variance $\sigma_N^{(2)}$ ($\sigma_N^{(1)}$).

V. INCORPORATING MEASUREMENT IMPERFECTIONS INTO THE GG02 CV-QKD PROTOCOL

In this section, we apply our results on asymmetric measurements to analyze the Gausssian modulated coherent state (GMCS, or GG02 [1]) CV-QKD protocol. Specifically, we compute the mutual information, Holevo information, and asymptotic secret key fraction under an untrusted noise scenario, in order to assess the impact of measurement asymmetry on the protocol's security.

In the GG02 protocol, Alice prepares an ensemble of coherent states whose complex amplitudes $\{\alpha = \frac{q+ip}{2}\}$ are drawn from a zero-mean Gaussian distribution, denoted by $G(0; V_A)$, where V_A is the modulation variance. Alice's preparation of coherent states can be understood as choosing random points in phase space whose coordinates (quadratures) are distributed according to a classical multivariate Gaussian probability distribution [36]:

$$
p_A(\alpha) = \frac{1}{\pi V_A} \exp\left(-\frac{|\alpha|^2}{V_A} \right)
\tag{69}
$$

After transmission through a Gaussian channel, which attenuates the coherent amplitude by a factor of $\sqrt{T}$, where T is the channel transmission, the state transforms as $|\alpha\rangle \mapsto |\sqrt{T}\alpha\rangle \equiv |\tilde{\alpha}\rangle$. Presense of channel noise with variance ξ further modifies the variance of the probability density function p_A as $V_A \mapsto TV_A + \xi$.

Then, Bob performs a measurement decribed by POVM $\{\hat{\Pi}_x\}$, where the index x parametrizes the measurement outcomes (e.g., quadrature values in homodyne detection). The conditional probability that Bob obtains measurement outcome x given that Alice sent the specific coherent state $|\tilde{\alpha}\rangle$ is given by the Born rule:

$$
p_B(x|\tilde{\alpha}) = \mathrm{Tr}\left[|\tilde{\alpha}\rangle\langle\tilde{\alpha}| \hat{\Pi}_x \right].
\tag{70}
$$

The joint probability distribution

$$
p_B(x, \tilde{\alpha}) = p_B(x|\tilde{\alpha}) p_A(\tilde{\alpha}),
\tag{71}
$$

and marginal distribution

$$
p_B(x) = \int \mathrm{d}^2\tilde{\alpha} \, p_B(x|\tilde{\alpha}) p_A(\tilde{\alpha}).
\tag{72}
$$

immediately follow.

Consider classical random vector $\mathbf{X} = (\alpha, x)^{\mathrm{T}}$, describing the joint classical variables involved in the protocol. We are able to calculate the classical covariance matrix as

$$
\mathrm{cov}\,(\mathbf{X}) = \Sigma^{\mathrm{HOM}} = \begin{pmatrix} V_A & \sqrt{T} V_A \\ \sqrt{T} V_A & V_B \end{pmatrix},
\tag{73}
$$

where the variance of Bob's measured quadrature is given by

$$
\mathrm{Var}(x) \equiv V_B = TV_A + 1 + \xi + \sigma_N
\tag{74}
$$

where σ_N is defined as per Eq. (24).

Mutual information between Alice and Bob can be calculated as follows [37]

$$
I_{AB}^{\mathrm{HOM}} = \frac{1}{2} \log \frac{V_A V_B}{\det \Sigma^{\mathrm{HOM}}} = \frac{1}{2} \log \frac{TV_A + 1 + \xi + \sigma_N}{1 + \xi + \sigma_N}.
\tag{75}
$$

where all logarithms are base 2.

To calculate mutual information if Bob performs double homodyne detection [2], we start from covariance matrix

$$
\Sigma_{AB} = \begin{pmatrix} V_A & \sqrt{T} V_A \\ \sqrt{T} V_A & TV_A + 1 + \xi \end{pmatrix} \equiv \begin{pmatrix} V_A & c \\ c & b \end{pmatrix},
\tag{76}
$$

note the difference in Bob's variance b as opposed to V_B – asymmetry noise would be modeled last, as it is not affected by beam splitter transformation. Bob's mode is splitted on BS_S, resulting in covariance matrix

$$\tilde{\Sigma}^{\text{DHOM}} = BS \left[\Sigma_{\text{AB}} \oplus \Sigma_{\text{vac}} \right] BS^T \tag{77}$$

where $\Sigma_{\text{vac}} = 1$ and $BS = 1 \oplus \begin{pmatrix} C_S & S_S \\ -S_S & C_S \end{pmatrix}$. Finally, we will model the measurement noise as

$$\Sigma^{\text{DHOM}} = \tilde{\Sigma}^{\text{DHOM}} + 0 \oplus N, \tag{78}$$

where

$$N = \begin{pmatrix} \sigma_N^{(1)} & 0 \\ 0 & \sigma_N^{(2)} \end{pmatrix} \tag{79}$$

where $\sigma_N^{(i)}$ is defined per Eq. (50).

The resulting covariance matrix describing measurement statistics in double homodyne detection reads

$$\Sigma^{\text{DH}} =$$
$$\begin{pmatrix} V_A & C_S c & -S_S c \\ C_S c & C_S^2 b + S_S^2 + \sigma_N^{(1)} & C_S S_S (1-b) \\ -S_S c & C_S S_S (1-b) & S_S^2 b + C_S^2 + \sigma_N^{(2)} \end{pmatrix}$$
$$\equiv \begin{pmatrix} V_A & \gamma_1 & \gamma_2 \\ \gamma_1 & \beta_1 & \gamma_{12} \\ \gamma_2 & \gamma_{12} & \beta_2 \end{pmatrix}, \tag{80}$$

which is then used to calculate mutual information between Alice and Bob

$$I = \frac{1}{2} \sum_i \log \frac{V_A \beta_i}{V_A \beta_i - \gamma_i^2}, \tag{81}$$

resulting in final formula

$$I = \frac{1}{2} \sum_i \log \frac{TV_i + \xi_i + 1 + \sigma_N^{(i)}}{\xi_i + 1 + \sigma_N^{(i)}}, \tag{82}$$

$$V_1 = C_S^2 V_A, \quad \xi_1 = C_S^2 \xi \tag{83}$$
$$V_2 = S_S^2 V_A, \quad \xi_2 = S_S^2 \xi. \tag{84}$$

Let us consider the generalization of double homodyne POVM presented in previous section. The covariance matrix of measurement's noise in this case relates to N from Eq. (79) as follows

$$N^{\text{sq}}(r) = S(r) N S(r), \tag{85}$$

where $S(r) = \text{diag}(e^r, e^{-r})$ is the squeezing transformation. This is equivalent with using noise variances from Eq. (68). Covariance matrix describing the state shared by Alice and Bob (see Eq. (77)) in squeezed states basis is given by

$$\tilde{\Sigma}^{\text{sq}} = \left[\mathbb{I} \oplus S(r) \right] \tilde{\Sigma}^{\text{DHOM}} \left[\mathbb{I} \oplus S(r) \right], \tag{86}$$

so the resulting total covariance matrix reads

$$\Sigma^{\text{sq}} = \begin{pmatrix} V_A & \gamma_1 e^{-r} & \gamma_2 e^r \\ \gamma_1 e^{-r} & \beta_1 e^{-2r} & \gamma_{12} \\ \gamma_2 e^r & \gamma_{12} & \beta_2 e^{2r} \end{pmatrix}, \tag{87}$$

dependency on r factors out, resulting in Eq. (81) and, consequently, Eq. (82).

To calculate Holevo information, first, consider two mode squeezed vacuum state (TMSVS), in ket notation written as [38]

$$|\Psi\rangle_{\text{AB}} = \sqrt{1 - \lambda^2} \sum_{n=0}^{\infty} (-\lambda)^n |n, n\rangle_{\text{AB}}, \tag{88}$$

where $\lambda = \tanh 2r$. Let Alice hold the state $\rho_{\text{AB}} = |\Psi\rangle_{\text{AB}} \langle \Psi|_{\text{AB}}$. In the entanglement based (EB) protocol, Alice measures one mode using a double measurement, which corresponds to a POVM of coherent state projectors $\left\{ \hat{\Pi}_\alpha = \frac{|\alpha\rangle\langle\alpha|}{\pi} \right\}$, and sends the second mode to Bob. The probability that Alice observes double homodyne outcome α is given by the Born rule:

$$p_A^{\text{DH}}(\alpha) = \text{Tr} \, \hat{\Pi}_\alpha \rho_A \tag{89}$$

where $\rho_A = \text{Tr}_B \, \rho_{\text{AB}}$ is the reduced density matrix of Alice's mode. Straightforward calculations lead to the expression of the reduced matrix as

$$\rho_A = \sum_n \frac{\bar{n}^n}{(\bar{n} + 1)^{n+1}} |n\rangle\langle n|, \tag{90}$$

where the mean number of photons $\bar{n} = \sinh^2 r = V_A$. It can be rewritten as [39]

$$\rho_A = \frac{1}{\pi \bar{n}} \int d^2\beta \, e^{-\frac{|\beta|^2}{\bar{n}}} |\beta\rangle\langle\beta|. \tag{91}$$

Substituing Eq. (91) into Eq. (89) yields

$$p_A^{\text{DH}}(\alpha) = \frac{1}{\pi (V_A + 1)} \exp \left[-\frac{|\alpha|^2}{V_A + 1} \right]. \tag{92}$$

After Alice obtains outcome α, second mode before channel transmission reads

$$\rho_B^\alpha = \frac{\text{Tr}_A \left[\hat{\Pi}_\alpha \otimes \mathbb{I} \right] \rho_{AB}}{p_A^{\text{DH}}(\alpha)} = |-\lambda \alpha^*\rangle\langle-\lambda \alpha^*|, \tag{93}$$

i.e. scaled coherent state. As channel simply multiplies the coherent amplitude by factor of $\sqrt{T}$, the conditional probability density distribution on Bob's side reads

$$p_B^{\text{DH}}(x|\tilde{\alpha}) = \text{Tr} \left[|-\lambda \tilde{\alpha}\rangle\langle-\lambda \tilde{\alpha}| \hat{\Pi}_x \right], \tag{94}$$

and joint probability distribution

$$p_B^{\text{DH}}(x, \tilde{\alpha}) = p_B^{\text{DH}}(x|\tilde{\alpha}) p_A^{\text{DH}}(\tilde{\alpha}). \tag{95}$$

As $V_A = \sinh^2 r$, we obtain the scaling factor λ as

$$\lambda = \frac{2\sqrt{V_A(V_A+1)}}{1+2V_A}. \tag{96}$$

With scaling by λ, as well as defining $V = V_A + 1$, the joint probability distribuion in entaglement based protocol Eq. (95) is exactly the same joint probability distribution in prepare and measure protocol Eq. (70).

It follows that the EB protocol reproduces the PM protocol probabilities. And so, calculation of Holevo information can be done from the covariance matrix of TMSVS in the form [40]

$$\Sigma_{AB}^{TVMS} =$$
$$\begin{pmatrix} (V_A+1)\mathbb{I} & \sqrt{T((V_A+1)^2-1)}\sigma_Z \\ \sqrt{T((V_A+1)^2-1)}\sigma_Z & V_B\mathbb{I} \end{pmatrix} \equiv$$
$$\begin{pmatrix} \alpha\mathbb{I} & \gamma\sigma_Z \\ \gamma\sigma_Z & V_B\mathbb{I} \end{pmatrix} \tag{97}$$

where the identity matrix is $\mathbb{I} = \mathrm{diag}(1,1)$, and $\sigma_Z = \mathrm{diag}(1,-1)$. If homodyne detection is used, Eve's entropy, $S_E = S_{AB}$, is calculated from the symplectic eigenvalues of Σ_{AB}^{TVMS} as [38]

$$\nu_{1,2}^{HOM} = \frac{1}{2}(z \pm [V_B - \alpha]),$$
$$z = \sqrt{(\alpha + V_B)^2 - 4\gamma^2}. \tag{98}$$

Bob's partial measurement of a single quadrature, described by the matrix $\Pi_{q,p}$, where $\Pi_q = \mathrm{diag}(1,0)$ and $\Pi_p = \mathrm{diag}(0,1)$ are measurements of $\hat{q}$ and $\hat{p}$ quadratures, respectively, transforms Alice's state covariance matrix as [40]

$$\Sigma_{A|B}^{HOM} = \alpha\mathbb{I} - \gamma^2 \sigma_Z [\Pi_{q,p}\, b\mathbb{I}\, \Pi_{q,p}]^{-1}\sigma_Z^T$$
$$= \alpha\mathbb{I} - \frac{\gamma^2}{b}\Pi_{q,p}. \tag{99}$$

The corresponding symplectic eigenvalue ν_3^{HOM} of $\Sigma_{A|B}$ is

$$\nu_3^{HOM} = \sqrt{\alpha\left(\alpha - \frac{\gamma^2}{b}\right)} \tag{100}$$

which allows us to calculate the conditional entropy $S_{E|B} = S_{A|B}$.

If double homodyne detection is used, Eve's entropy S_E is calculated using the symplectic eigenvalues of the covariance matrix

$$\Sigma_{AB}^{DHOM} = \begin{pmatrix} \alpha\mathbb{I} & \gamma\sigma_Z \\ \gamma\sigma_Z & V_B^{DHOM}\mathbb{I} \end{pmatrix}, \tag{101}$$

where $V_B^{DHOM} = TV_A + \xi + \frac{\sigma_1+\sigma_2}{2}$.

Double homodyne detection of Bob's mode transforms Alice's conditional covariance matrix as

$$\Sigma_{A|B}^{DHOM} = \alpha\mathbb{I} - \gamma^2\sigma_Z[b\mathbb{I} + \mathbb{I}]^{-1}\sigma_Z^T$$
$$= \left(\alpha - \frac{\gamma^2}{b+1}\right)\mathbb{I}, \tag{102}$$

resulting in symplectic eigenvalue ν_3^{DHOM} in the form

$$\nu_3^{DHOM} = \alpha - \frac{\gamma^2}{b+1}. \tag{103}$$

The Holevo information is calculated as

$$\chi_{EB} \equiv S_E - S_{E|B} = S_{AB} - S_{A|B}$$
$$= \sum_{i=1,2} g(\nu_i) - g(\nu_3), \tag{104}$$

where

$$g(\nu) = \frac{\nu+1}{2}\log\frac{\nu+1}{2} - \frac{\nu-1}{2}\log\frac{\nu-1}{2}, \tag{105}$$

with appropriate substitution of ν_i depending on the measurement scheme, and the asymptotic secret fraction is then calculated as

$$R = \beta I_{AB} - \chi_{EB}, \tag{106}$$

where β is the reconciliation efficiency.

The effects of detection asymmetry on mutual information, Holevo information, and the asymptotic secret key rate are illustrated in Fig. 9 for homodyne detection and Fig. 10 for double homodyne detection. Our numerical results for the homodyne case are consistent with Ref. [24], namely the dependency of asymptotic secret fraction on beam splitter deviation. The dependence of the asymptotic secret key rate on channel length in the presence of asymmetrical detection is shown in Fig. 11. These results indicate that in the untrusted noise scenario, asymmetrical homodyne detection does not offer any advantage, as ideal detection minimizes Holevo information, while double homodyne detection consistently yields better performance.

VI. CONCLUSION AND DISCUSSION

In this paper, we have studied the effects of asymmetry introduced by unbalanced beam splitters and different efficiencies of the photodetectors in photocount statistics of homodyne and double homodyne detection. We have performed numerical analysis to explore the applicability range for the Gaussian approximation derived by approximating the Poisson distributions using the probability density functions of normally distrbuted random variables.

By using the Gaussian approximation, we have developed the method for constructing POVMs of homodyne-based schematics. This method is applied to deduce the expression for the POVM that generalizes the well-known results to the case of the asymmetric homodyne detection. This POVM is found to be well defined across all parameter settings of the scheme with the excess noise variance modified by the asymmetry and incorporates the effect of asymmetry-induced shift of the mean value (these effects are illustrated in Fig. 4).

(a) I_{AB}
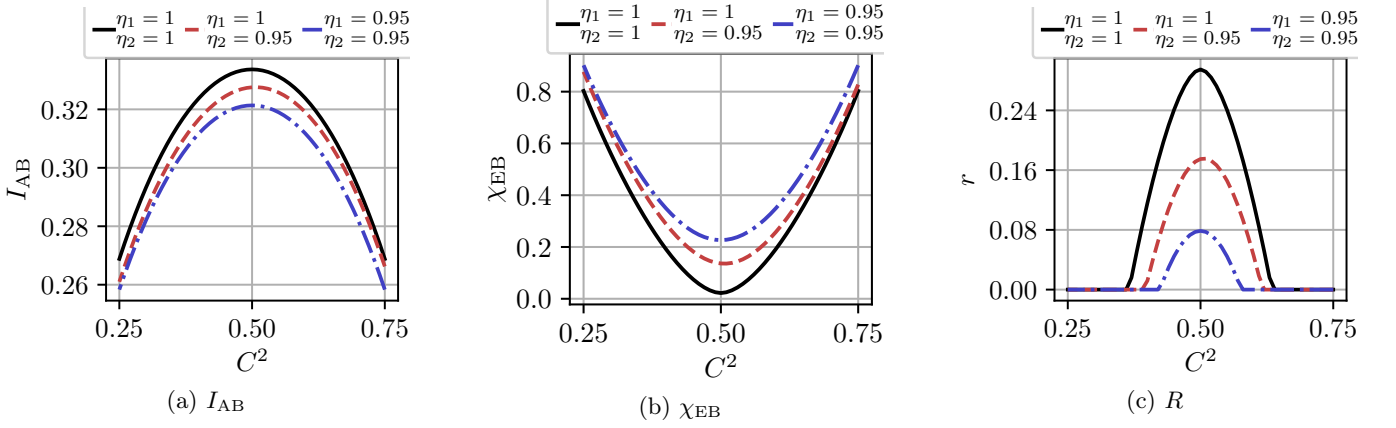
(b) χ_{EB}

(c) R

Figure 9: (a) Mutual information, (b) Holevo information, and (c) asymptotic secret fraction using homodyne measurement as functions of the beam splitter transmission, for various detector efficiencies at $V = 1, T = 0.95, \xi = 10^{-3}, \beta = 0.95$

(a) I_{AB}
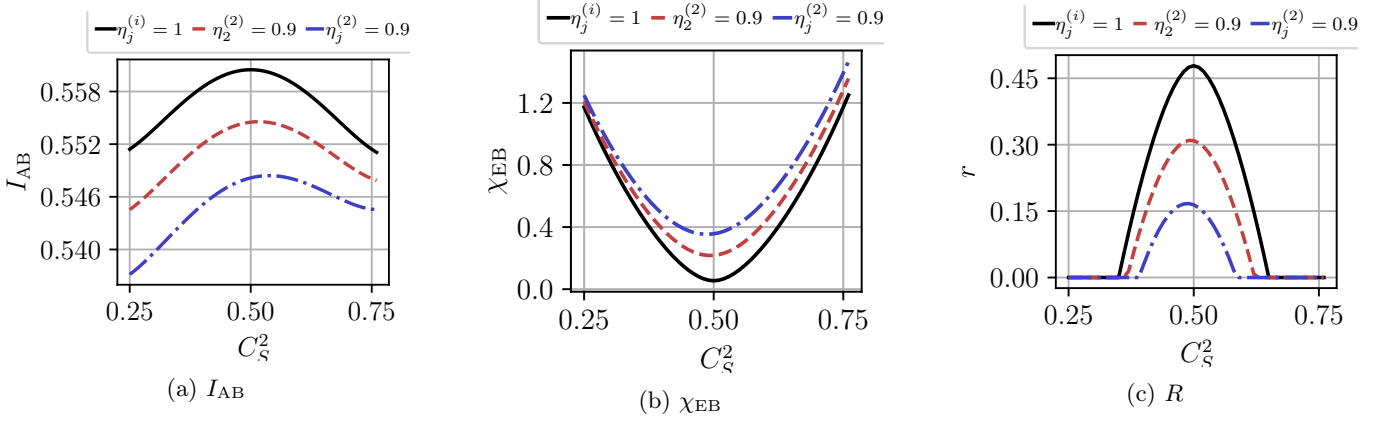
(b) χ_{EB}

(c) R

Figure 10: (a) Mutual information, (b) Holevo information, and (c) asymptotic secret fraction using double homodyne detection as functions of the signal beam splitter transmission. All other beam splitters are assumed to be balanced. Results are shown for various detector efficiencies; efficiencies not specified in the legend are taken to be unity. Parameters: $V = 1, T = 0.95, \xi = 10^{-3}, \beta = 0.95$.

We have used the total variational distance (27), D_P, to quantify the statistical distance between the Skellam and Gaussian distributions and evaluate the accuracy of the Gaussian approximation across various asymmetry parameters. It is found that, for the signal mode prepared in the coherent state $|\alpha\rangle$, the distance increases with $|\alpha|$ (see Fig. 2a) and, in the small-amplitude region with $|\alpha| \leq 0.1$, the maximum value of the distance can be estimated at about 0.13 reached when the local oscillator amplitude $|\alpha_L|$ is in the vicinity of unity. At $|\alpha_L| > 1$, the distance rapidly drops with the LO amplitude. For example, at $|\alpha| = 0.5$, the distance falls below 0.05 when the ratio $|\alpha_L|/|\alpha|$ exceeds five (see Fig. 2b).

We have found that (see Figs. 3 and 5) dependence of the distance on the photodetector efficiencies (the disbalance angle of the beam splitter) is sensitive to the disbalance of the beam splitter (photodetector efficiencies). Thus, by varying parameters of BS we may achieve the

best approximation for given quantum efficiencies and vice versa. In general, our findings indicate that the quality of the agreement between the exact and approximate photocount distributions varies with the degree of asymmetry.

Our formalism allows us to easily analyze various homodyne-based schematics. It can be extended to describe more complex measurement systems. We have demonstrated this by performing an analysis for the eight-port asymmetric double homodyne scheme. For this scheme, we have deduced the Gaussian approximation (see Eqs. (38)– (40)) and the corresponding POVM expressed in terms of the projectors onto coherent states (see Eq. (51)). As is shown in Fig. 7, the asymmetry induces effects such as shifts and anisotropy of the distributions in the photocount difference plane.

As shown in the main text, the applicability of double homodyne POVM in the form (51) may be broken pro-

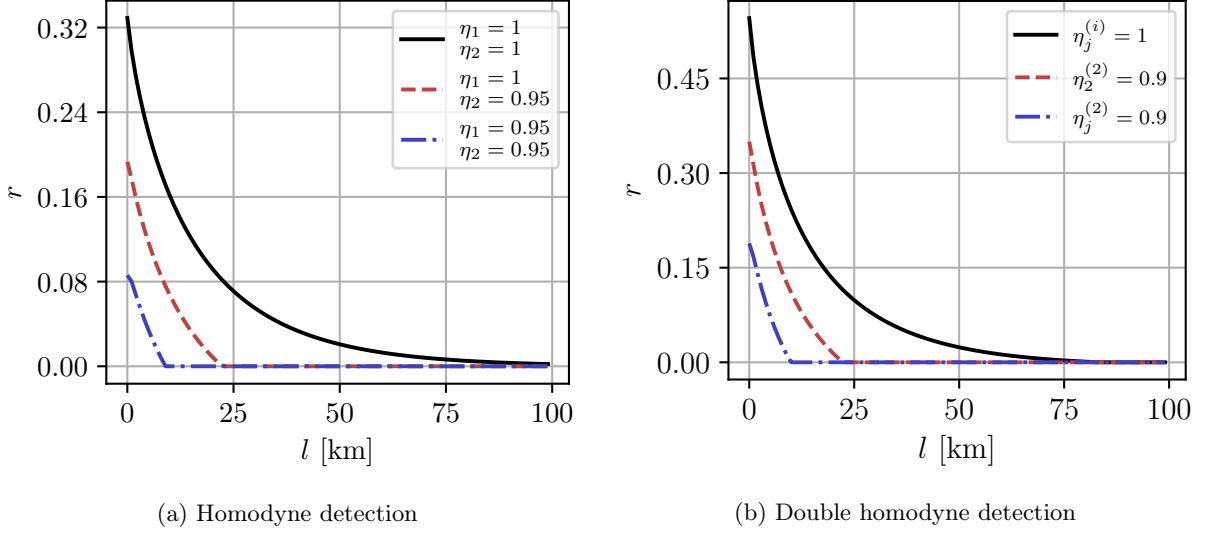(a) Homodyne detection

(b) Double homodyne detection

Figure 11: Asymptotic secret fraction as a function of channel length computed for (a) homodyne detection and (b) double homodyne detection, shown for various detector efficiencies. Parameters are $V = 1, T = 0.95, \xi = 10^{-3}, \beta = 0.95$. The losses are assumed to be 20 dB per 100 km.

vided that the beam splitter for the signal mode is unbalanced. To resolve this, an extension to the set of squeezed coherent states is needed (see Eq. (68)), leading to explicit dependency of POVM on the squeezing parameter, which is not defined unambiguously. This implies that there are, generally, infinitely many POVMs representing one set of the parameters of double homodyne scheme, and so the squeezing parameter needs additional rule to make the POVM well-defined. Practically, however, ambiguousness of POVM does not matter, as all of their averages represent the same photon counting difference statistical distribution (38) or, equivalently, quadrature distribution (41). This is supported by our calculations for mutual information between Alice and Bob in Gaussian modulated coherent states CV-QKD protocol (for a comprehensive review see, e.g., Ref. [40]). As we have shown, choosing any POVM in the form (68) would yield the same result for secret fraction, as it is dependent only on variances of quadrature distribution (41).

Generalization to complex transmission and reflection coefficients for both homodyne and double homodyne is trivial. For homodyne, this would entail changing the definition of ϕ in Eq. (13) to $\phi' \equiv \phi + \phi_t - \phi_r$, where ϕ_t and ϕ_r are phases of complex transmission and reflection coefficients, respectively, and the definition of quadrature variable (16) would remain unchanged. For double homodyne, introducing phases as $\phi_{r,t}^{(j)}, i \in \{1, 2, S, L\}$, a change of $\operatorname{Re} \alpha e^{-i\phi} \mapsto \operatorname{Re} \alpha e^{-i(\phi - \phi_t^{(L)} - \phi_t^{(S)})}$ and $\operatorname{Im} \alpha e^{-i\phi} \mapsto \operatorname{Im} \alpha e^{-i(\phi - \phi_r^{(L)} - \phi_r^{(S)})}$ is needed in Eq. (41), leaving quadrature variables (42), (43) unchanged if $\phi_r^{(1)} + \phi_t^{(1)} = \phi_r^{(2)} + \phi_t^{(2)} = 0$.

Note that, according to Appendix A, an alternative method based on the Gaussian approximation for the

Bessel function that enters the Skellam distribution generally leads to results that are not suitable for dealing with asymmetry-induced effects in homodyne detection.

Our concluding remark is to put our results in the context of CV-QKD [41]. The asymmetry effects described in the paper, such as deviations from the ideal 50:50 beam splitter ratio and mismatched detector efficiencies, introduce vulnerabilities into CV-QKD systems. These vulnerabilities can be exploited by adversaries through attack strategies such as the wavelength attack [42, 43] and the homodyne detector blinding [44] and saturation [45]. The wavelength attack leverages the wavelength-dependent coupling ratio of fiber beam splitters and can be countered by using proper spectral filtering. Blinding and saturation attacks exploit the saturation behavior of homodyne detectors, and their effectiveness is amplified by receiver imbalance. If the splitting ratio deviates from ideal one, an injected bright pulse more easily displaces the detector output, facilitating saturation and biasing excess noise estimation.

In the main text, we analyzed how measurement asymmetry impacts the performance of CV-QKD system in the untrusted noise scenario, where asymmetry noise is accessible to Eve. In this case, even relatively small asymmetry significantly reduces maximum channel length (see Fig. 11). In trusted-noise CV-QKD [46], if Alice and Bob are unaware of detector's arms asymmetry, they may misinterpret the increased variance as channel excess noise rather than trusted detector imperfection. This leads to an overestimation of channel excess noise and an underestimation of trusted detector noise. Similar to blinding attacks, this vulnerability can be mitigated by inserting attenuators to balance the detection scheme.

Appendix A: Gaussian approximation from Skellam distribution

The derivation procedure for the Gaussian approximation outlined in Sec. II A transforms the photocount difference probability (6) into the form of a convolution of the normal distributions by approximating the Poisson distributions. In this Appendix, we discuss an alternative method where the starting point is the Skellam distribution (7). For convenience, we shall reproduce the expression for this distribution here:

$$P(\mu) = e^{-\eta_1|\alpha_1|^2} e^{-\eta_2|\alpha_2|^2} \left(\frac{\eta_1|\alpha_1|^2}{\eta_2|\alpha_2|^2}\right)^{\frac{\mu}{2}}$$
$$\times I_\mu\left(2\sqrt{\eta_1\eta_2|\alpha_1|^2|\alpha_2|^2}\right), \tag{A1}$$

where $I_k(z)$ is the modified Bessel function of the first kind and the amplitudes $|\alpha_{1,2}|$ are given by Eq. (3).

The method under consideration (see, e.g. the textbook [30]) assumes that, in the strong LO limit, the argument of the modified Bessel function is large and $I_\mu(z)$ can be approximated using its asymptotic expansion taken in the Gaussian form:

$$I_\mu(z) \approx \frac{1}{\sqrt{2\pi z}} \exp\left[z - \frac{\mu^2}{2z}\right]. \tag{A2}$$

This formula can be deduced by performing a saddle-point analysis for the integral representation of the Bessel functions [22].

Heuristically, it can also be obtained from from the lowest order asymptotic expansion for the Bessel function [29]: $I_\mu(z) \approx e^z(1 - (4\mu^2 - 1)/(8z))/\sqrt{2\pi z}$ assuming that, for small values of x, $1 - x$ can be replaced with e^{-x} (the factors independent of μ are not essential because they can be incorporated into the normalization factor of the Gaussian approximation).

Assuming that $CS \neq 0$ and $|\alpha_L|$ is sufficiently large, we can use the approximate relations

$$z = 2\sqrt{\eta_1\eta_2}|\alpha_1||\alpha_2| \approx 2CS\sqrt{\eta_1\eta_2}|\alpha_L|^2, \tag{A3}$$

$$\ln\left(\frac{\eta_1|\alpha_1|^2}{\eta_2|\alpha_2|^2}\right)^{\frac{\mu}{2}} \approx \frac{\mu}{2}\left(\ln\frac{\eta_1 S^2}{\eta_2 C^2} + \frac{\langle\hat{x}_\phi\rangle}{CS|\alpha_L|}\right) \tag{A4}$$
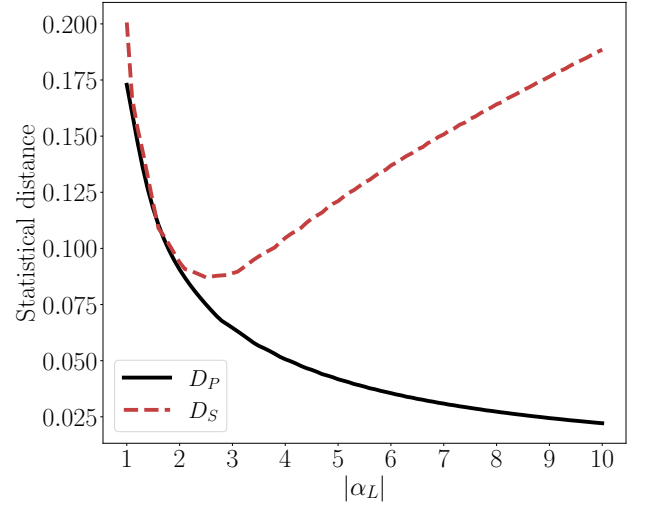

Figure 12: Distances, $D_P = D(\mathsf{P}, \mathsf{P}_G)$ and $D_S = D(P, \mathsf{P}_G^{(s)})$, between the Skellam distribution, P, and two Gaussian approximations, P_G (see Eq. (10)) and $\mathsf{P}_G^{(s)}$ (see Eq. (A5)), as a function of $|\alpha_L|$ the beam splitter disbalance angle at $\delta\theta = 15°$ $\alpha = 1$, and $\eta_1 = \eta_2 = 1$.

to obtain the Gaussian approximation for the Skellam distribution (A1) given by

$$\mathsf{P}_G^{(s)}(\mu) = G(\mu - \tilde{\mu}_G; \tilde{\sigma}_G), \tag{A5}$$

$$\tilde{\mu}_G = \sqrt{\eta_1\eta_2}\left[CS|\alpha_L|^2 \ln\frac{\eta_1 S^2}{\eta_2 C^2} + |\alpha_L|\langle\hat{x}_\phi\rangle\right], \tag{A6}$$

$$\tilde{\sigma}_G = 2CS\sqrt{\eta_1\eta_2}|\alpha_L|^2. \tag{A7}$$

Similar to Eq. (15), we cast the probabilty (A5) into the following quadrature form:

$$\mathsf{P}_G^{(s)}(\tilde{x}) = \frac{1}{\sqrt{2\pi}\tilde{\sigma}_G} \exp\left\{-\frac{(\tilde{x} - \langle\hat{x}_\phi\rangle)^2}{2\tilde{\sigma}_x}\right\}, \tag{A8}$$

$$\tilde{x} = \frac{\mu}{\sqrt{\eta_1\eta_2}|\alpha_L|} - CS|\alpha_L| \ln\frac{\eta_1 S^2}{\eta_2 C^2}, \tag{A9}$$

$$\tilde{\sigma}_x = \frac{2CS}{\sqrt{\eta_1\eta_2}}, \tag{A10}$$

so that we may follow the line of reasoning presented in Sec. II A to deduce the POVM

$$\hat{\Pi}_G^{(s)} = \frac{1}{\sqrt{\eta_1\eta_2}|\alpha_L|}$$
$$\times \int \mathrm{d}x' G(x - x'; \tilde{\sigma}_N)|x', \phi\rangle\langle x', \phi| \tag{A11}$$

with the noise variance

$$\tilde{\sigma}_N = \tilde{\sigma}_x - 1, \quad 0 \leq \tilde{\sigma}_x \leq \tilde{\sigma}_x^{(\max)} = 1/\sqrt{\eta_1\eta_2}. \tag{A12}$$

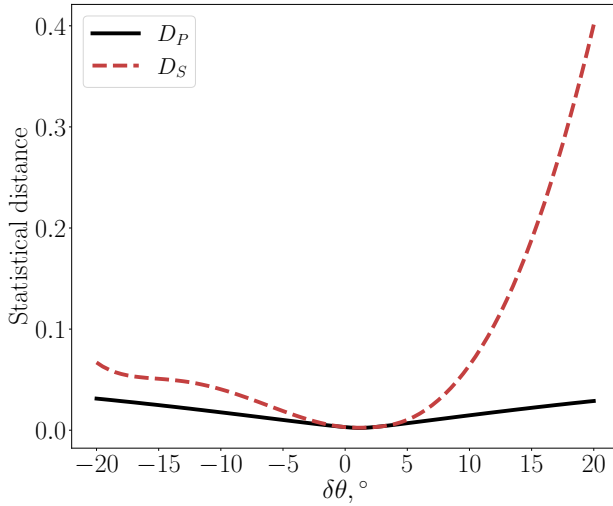Note that, in the symmetric case with $C = S$ and $\eta_1 = \eta_2$, the Gaussian distributions given by Eqs. (10)

Figure 13: Distances, $D_P = D(\mathsf{P}, \mathsf{P}_G)$ and $D_S = D(\mathsf{P}, \mathsf{P}_G^{(s)})$, between the Skellam distribution, P, and two Gaussian approximations, P_G (see Eq. (10)) and $\mathsf{P}_G^{(s)}$ (see Eq. (A5)), as a function of the beam splitter disbalance angle $\delta\theta$ at $\alpha = 1$, $\alpha_L = 10$ and $\eta_1 = \eta_2 = 1$.

and (A5) are equivalent. This is no longer the case in the presence of asymmetry effects.

Figure 12 demonstrates that, at $\delta\theta \neq 0$, by contrast to the distance between P and P_G, $D_P = \mathsf{D}(\mathsf{P}, \mathsf{P}_G)$ which is a monotonically decreasing function of $|\alpha_L|$, the distance between the Skellam distribution and the approximate distribution (A5), $D_S = \mathsf{D}(\mathsf{P}, \mathsf{P}_G^{(s)})$, reveals non-monotonic behaviour and increases with $|\alpha_L|$ at sufficiently large LO amplitudes. Referring to Fig. 13, disbalance of the beam splitter has strong detrimental effect on the accuracy of the approximation (A5).

What is more important is that, by contrast the noise excess variance (24) which is always positive, the variance (A12) becomes negative when $2CS \leq \sqrt{\eta_1\eta_2}$. The latter breaks applicability of Eq. (A11) giving an ill-posed POVM.

[1] F. Grosshans and P. Grangier, Continuous variable quantum cryptography using coherent states, Phys. Rev. Lett. **88**, 057902 (2002).

[2] C. Weedbrook, A. M. Lance, W. P. Bowen, T. Symul, T. C. Ralph, and P. K. Lam, Quantum cryptography without switching, Phys. Rev. Lett. **93**, 170504 (2004).

[3] C. Weedbrook, S. Pirandola, R. García-Patrón, N. J. Cerf, T. C. Ralph, J. H. Shapiro, and S. Lloyd, Gaussian quantum information, Rev. Mod. Phys. **84**, 621 (2012).

[4] E. Diamanti and A. Leverrier, Distributing secret keys with quantum continuous variables: Principle, security and implementations, Entropy **17**, 6072 (2015).

[5] R. Goncharov, I. Vorontsova, D. Kirichenko, I. Filipov, I. Adam, V. Chistiakov, S. Smirnov, B. Nasedkin, B. Pervushin, D. Kargina, E. Samsonov, and V. Egorov, The rationale for the optimal continuous-variable quantum key distribution protocol, Optics **3**, 338 (2022).

[6] Y. Zhang, Y. Bian, Z. Li, S. Yu, and H. Guo, Continuous-variable quantum key distribution system: Past, present, and future, Applied Physics Reviews **11**, 011318 (2024).

[7] W. Vogel, Homodyne correlation measurements with weak local oscillators, Phys. Rev. A **51**, 4160 (1995).

[8] B. L. Schumaker, Noise in homodyne detection, Opt. Lett. **9**, 189 (1984).

[9] H. P. Yuen and V. W. S. Chan, Noise in homodyne and heterodyne detection, Opt. Lett. **8**, 177 (1983).

[10] G. L. Abbas, V. W. S. Chan, and T. K. Yee, Local-oscillator excess-noise suppression for homodyne and heterodyne detection, Opt. Lett. **8**, 419 (1983).

[11] S. Wallentowitz and W. Vogel, Unbalanced homodyning for quantum state measurements, Phys. Rev. A **53**, 4528 (1996).

[12] G. S. Thekkadath, D. S. Phillips, J. F. F. Bulmer, W. R. Clements, A. Eckstein, B. A. Bell, J. Lugani, T. A. W. Wolterink, A. Lita, S. W. Nam, T. Gerrits, C. G. Wade, and I. A. Walmsley, Tuning between photon-number and quadrature measurements with weak-field homodyne detection, Phys. Rev. A **101**, 031801 (2020).

[13] J. Sperling, W. Vogel, and G. S. Agarwal, True photocounting statistics of multiple on-off detectors, Phys. Rev. A **85**, 023820 (2012).

[14] T. Lipfert, J. Sperling, and W. Vogel, Homodyne detection with on-off detector systems, Phys. Rev. A **92**, 053835 (2015).

[15] A. Cives-Esclop, A. Luis, and L. L. Sánchez-Soto, An eight-port detector with a local oscillator of finite intensity, Journal of Optics B: Quantum and Semiclassical Optics **2**, 526 (2000).

[16] J. Combes and A. P. Lund, Homodyne measurement with a schrödinger cat state as a local oscillator, Physical Review A **106**, 063706 (2022).

[17] J.-Y. Haw, S. Assad, A. Lance, N. Ng, V. Sharma, P. K. Lam, and T. Symul, Maximization of extractable randomness in a quantum random-number generator, Physical Review Applied **3**, 054004 (2015).

[18] A. A. Hajomer, A. N. Oruganti, I. Derkach, U. L. Andersen, V. C. Usenko, and T. Gehring, Finite-size security of continuous-variable quantum key distribution with imperfect heterodyne measurement, arXiv preprint arXiv:2501.10278 (2025).

[19] V. Y. Len, M. Byelova, V. Uzunova, and A. Semenov, Realistic photon-number resolution in generalized hong-ou-mandel experiment, Physica Scripta **97**, 105102 (2022).

[20] I. Yeremenko, M. Dmytruk, and A. Semenov, Realistic photon-number resolution in gaussian boson sampling, Physical Review A **110**, 043715 (2024).

[21] A. Reutov and D. Sych, Photon counting statistics with imperfect detectors, in *Journal of Physics: Conference Series*, Vol. 2086 (IOP Publishing, 2021) p. 012096.

[22] M. Freyberger, K. Vogel, and W. P. Schleich, From photon counts to quantum phase, Physics Letters A **176**, 41 (1993).

[23] S. Olivares, A. Allevi, and M. Bondani, On the role of the local oscillator intensity in optical homodyne-like tomography, Physics Letters A **384**, 126354 (2020).

[24] A. Ruiz-Chamorro, D. Cano, A. Garcia-Callejo, and V. Fernandez, Effects of experimental impairments on the security of continuous-variable quantum key distribution, Heliyon **9** (2023).

[25] S. Pirandola, U. L. Andersen, L. Banchi, M. Berta, D. Bunandar, R. Colbeck, D. Englund, T. Gehring, C. Lupo, C. Ottaviani, J. L. Pereira, M. Razavi, J. S. Shaari, M. Tomamichel, V. C. Usenko, G. Vallone, P. Villoresi, and P. Wallden, Advances in quantum cryptography, Adv. Opt. Photon. **12**, 1012 (2020).

[26] P. L. Kelley and W. H. Kleiner, Theory of electromagnetic field measurement and photoelectron counting, Phys. Rev. **136**, A316 (1964).

[27] W. Vogel and J. Grabow, Statistics of difference events in homodyne detection, Phys. Rev. A **47**, 4227 (1993).

[28] J. G. Skellam, The frequency distribution of the difference between two poisson variates belonging to different populations, Journal of the Royal Statistical Society Series A: Statistics in Society **109**, 296 (1946).

[29] F. W. J. Olver, D. W. Lozier, R. F. Boisvert, and C. W. Clark, eds., *NIST Handbook of Mathematical Functions* (NIST & Cambridge University Press, New York, 2010) p. 951.

[30] W. Vogel and D.-G. Welsch, *Quantum Optics*, 3rd ed. (Wiley-VCH, Berlin, 2006) p. 508.

[31] P. Lahti, J.-P. Pellonpää, and J. Schultz, Realistic eight-port homodyne detection and covariant phase space observables, Journal of Modern Optics **57**, 1171 (2010).

[32] T. Richter, Double homodyne detection and quantum state determination, in *European Quantum Electronics Conference* (Optica Publishing Group, 1998) p. QTuG38.

[33] A. Leverrier, Security of continuous-variable quantum key distribution via a gaussian de finetti reduction, Phys. Rev. Lett. **118**, 200501 (2017).

[34] C. Gerry and P. Knight, *Introductory Quantum Optics* (Cambridge University Press, NY, 2005) p. 317.

[35] M. G. Genoni, S. Mancini, and A. Serafini, General-dyne unravelling of a thermal master equation, Russian Journal of Mathematical Physics **21**, 329 (2014).

[36] A. Serafini, *Quantum Continuous Variables: A Primer of Theoretical Methods* (CRC Press, Taylor & Francis Group, Boca Raton, 2017) p. 350.

[37] J. Soch *et al.*, Statproofbook/statproofbook.github.io: The book of statistical proofs (version 2023), `https://doi.org/10.5281/zenodo.4305949` (2024), accessed: 2025-07-15.

[38] C. Weedbrook, S. Pirandola, R. García-Patrón, N. J. Cerf, T. C. Ralph, J. H. Shapiro, and S. Lloyd, Gaussian quantum information, Rev. Mod. Phys. **84**, 621 (2012).

[39] M. O. Scully and M. S. Zubairy, *Quantum Optics* (Cambridge University Press, Cambridge, 1997) p. 630.

[40] F. Laudenbach, C. Pacher, C.-H. F. Fung, A. Poppe, M. Peev, B. Schrenk, M. Hentschel, P. Walther, and H. Hübel, Continuous-variable quantum key distribution with gaussian modulation—the theory of practical implementations, Advanced Quantum Technologies **1**, 1800011 (2018).

[41] Y. Zhang, Y. Bian, Z. Li, S. Yu, and H. Guo, Continuous-variable quantum key distribution system: Past, present, and future, Applied Physics Reviews **11** (2024).

[42] J.-Z. Huang, Z.-Q. Yin, S. Wang, H.-W. Li, W. Chen, G.-C. Guo, and Z.-F. Han, Wavelength attack scheme on continuous-variable quantum key distribution system using heterodyne detection protocol, arXiv preprint arXiv:1206.6550 (2012).

[43] J.-Z. Huang, S. Kunz-Jacques, P. Jouguet, C. Weedbrook, Z.-Q. Yin, S. Wang, W. Chen, G.-C. Guo, and Z.-F. Han, Quantum hacking on quantum key distribution using homodyne detection, Physical Review A **89**, 032304 (2014).

[44] H. Qin, R. Kumar, V. Makarov, and R. Alléaume, Homodyne-detector-blinding attack in continuous-variable quantum key distribution, Physical Review A **98**, 012312 (2018).

[45] H. Qin, R. Kumar, and R. Alléaume, Quantum hacking: Saturation attack on practical continuous-variable quantum key distribution, Physical Review A **94**, 012325 (2016).

[46] V. C. Usenko and R. Filip, Trusted noise in continuous-variable quantum key distribution: a threat and a defense, Entropy **18**, 20 (2016).